Effects of Jamming and Excision Filtering
Upon Error Rates and Detectability
of a Spread Spectrum Communications System

THESIS
Christopher B. Madden
2nd Lieutenant, USAF

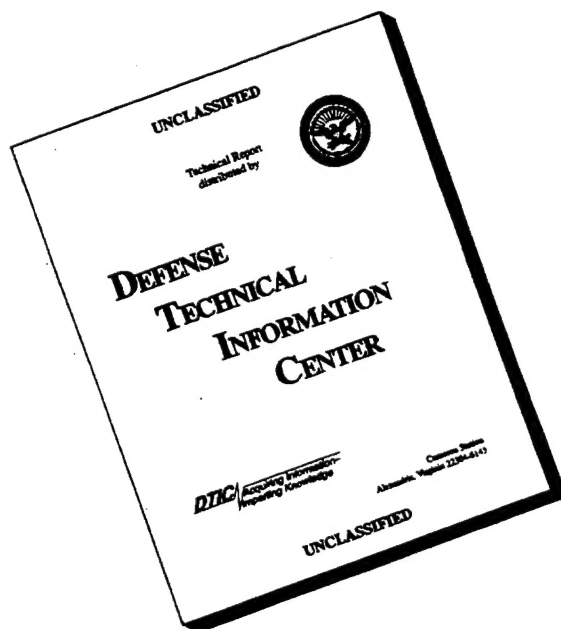AFIT/GE/ENG/95D-13

19960327 006

DEPARTMENT OF THE AIR FORCE
AIR UNIVERSITY
AIR FORCE INSTITUTE OF TECHNOLOGY

Wright-Patterson Air Force Base, Ohio

DTIC QUALITY INSPECTED 1

DISCLAIMER NOTICE

UNCLASSIFIED

Technical Report
distributed by

**DEFENSE
TECHNICAL
INFORMATION
CENTER**

DTIC Acquiring Information-
Imparting Knowledge

Cameron Station
Alexandria, Virginia 22304-6145

UNCLASSIFIED

THIS DOCUMENT IS BEST
QUALITY AVAILABLE. THE
COPY FURNISHED TO DTIC
CONTAINED A SIGNIFICANT
NUMBER OF PAGES WHICH DO
NOT REPRODUCE LEGIBLY.

AFIT/GE/ENG/95D-13

Effects of Jamming and Excision Filtering
Upon Error Rates and Detectability
of a Spread Spectrum Communications System

THESIS
Christopher B. Madden
2nd Lieutenant, USAF

AFIT/GE/ENG/95D-13

Effects of Jamming and Excision Filtering

Upon Error Rates and Detectability

of a Spread Spectrum Communications System

THESIS

Presented to the Faculty of the School of Engineering

of the Air Force Institute of Technology

Air University

In Partial Fulfillment of the

Requirements for the Degree of

Master of Science in Electrical Engineering

Christopher B. Madden, B.S. Electrical Engineering

2nd Lieutenant, USAF

December 1995

Table of Contents

List of Figures

List of Tables

AFIT/GE/ENG/95D-13

Abstract

This thesis examines the effects of a digital excision filter (DEF) upon the error rates and detectability of a Direct-Sequence Binary Phase Shift Keyed communication signal in the presence of both continuous-wave (CW) and pulsed jammers. Simulations were performed using the Comdisco Signal Processing Worksystem. Detector models used were the wideband radiometer and two forms of the chip-rate detector. Twelve jamming scenarios were used to test the performance of the DEF in the presence of the CW and pulsed jammers. In addition, the effects of the CW jammer frequency, the pulsed jammer duty cycle, and the pulsed jammer PRF were also examined. LPI quality factors were then used to quantify the performance of the DEF.

This research determined that the DEF was able to remove almost 100% of the CW jammer and allowed the communication receiver and interceptors to operate with little degradation. The DEF was less effective against the pulsed jammers; however, it still allowed the receivers to operate at an acceptable level for single jammers. When two or more pulsed jammers were present, the radiometer was still able to operate; however, the other interceptors' performance was unacceptable.

Effects of Jamming and Excision Filtering Upon Error Rates and Detectability of a Spread Spectrum Communications System

I. Introduction

1.1 Background

The objective of any communication system is to transfer information between a transmitter and a receiver with a minimum amount of error. As these systems began to be used in military scenarios, it was inevitable that attempts would be made to disrupt or intercept this information. In order to prevent the enemy from accomplishing these objectives, many different methods have been used to conceal the information and to make it robust in the presence of interference. These attempts can be classified into two different categories. The first of these, information security (INFOSEC), deals with the means used to conceal the information content of the signal. INFOSEC does not care if the signal can be detected or intercepted. It is strictly concerned with preventing the interceptor from obtaining the information it contains. The main method used for accomplishing this goal is cryptography. By encrypting a message into a form which can not be deciphered, the objective of INFOSEC can be accomplished (12).

The second method used to prevent the exploitation or disruption of a communication signal is known as transmission security (TRANSEC). In this method, the focus is upon concealing the presence of the signal while also reducing the effects of hostile interference. By using communication systems which reduce the energy density of the transmitted signal, the probability that a signal will be detected and exploited will be dramatically decreased. Spread Spectrum (SS) communications is based upon this principle. By increasing the bandwidth over which a signal's energy is contained, the energy density of the signal is reduced. By using the minimum signal power and an optimum coding scheme, the probability of signal detection can be minimized (12) (17).

Spread Spectrum signals also have the added benefit of being less susceptible to jamming signals. Upon reception of the communication and jamming signals by the SS receiver, the coding process is

reversed and the energy density of the communication signal is returned to its original level. At the same time, the energy density of the jammer is reduced by the same factor. Because of these properties, of spread spectrum techniques are often employed in military communication systems.

In a typical military scenario, a communication system is often subjected to numerous interference sources. Because of this, the anti-jam benefits of the spreading process itself are often insufficient. This has resulted in the use of filtering in an attempt to remove the interference sources. However, the filtering that removes the interference also removes a portion of the desired communication signal. Therefore, the filtering method must remove the largest possible portion of the interference while maintaining the integrity of the original information. There are two main methods that can be used to achieve this objective. These are time-domain filters and transform-domain filters.

The most common time-domain filtering method is known as the estimator/subtracter method. This process attempts to estimate the interference signal and then subtract it from the received signal. This method is often difficult due to the replica generation process. It is necessary to estimate the frequency, amplitude, and phase of the interference source. If the interference is accurately replicated, significant reductions in jammer effectiveness can be achieved (13). Time-domain techniques work well as long as the interference bandwidth does not exceed ten percent of the spread spectrum bandwidth (5). Time-domain filters are also hampered by multiple jammers. When more than one jammer is present, it becomes increasingly more difficult to replicate the individual jammer signals.

The second method, transform-domain filtering, performs signal processing algorithms upon the Fourier transform of the received signal. After the processing, an inverse Fourier transform is taken and the output is passed on to the remainder of the receiver. One algorithm excises the frequency bins which exceed a specified threshold (11). Another algorithm used is to estimate the spectrum of the received signal in order to derive a whitening filter. This filter can then be used to remove the interference (13). The main concern with these methods is the processing time of the filter. If speeds are not adequate, the signal can be distorted. The transform-domain filters are capable of handling larger interference bandwidths; however, they are less effective when the jammer power is much larger than the signal power. Finally, another benefit of the transform-domain filters is their ability to handle multiple jammers (5).

1.2 Problem Statement

In an operational military communication system, the user is often concerned with the effective communication range that can be maintained in the presence of multiple interference sources and interceptors. These effects can be quantified through the use of the LPI quality factors which are discussed in Chapter III and Appendix A. This research will examine the effects of a transform-domain filter upon the modulation and interference suppression quality factors for a direct sequence spread spectrum binary phase shift keyed communication system. The performance of the filter in various jamming scenarios will be evaluated, and the quality factors will be examined as a function of jammer parameters. Finally, the effects of the filter upon the receiver operating characteristics of multiple interceptor models will be examined.

1.3 Assumptions

This research assumes that all communication channels can be modeled as a sum of additive white Gaussian noise and the jammer signals present in the various scenarios. It also assumes that code synchronization is maintained at the communication receiver, and that there is no propagation delay. Finally, it assumes that no multi-path propagation occurs.

1.4 Scope

The systems considered in this research consist of a basic direct sequence spread spectrum (DS-SS) binary phase shift keyed (BPSK) signal and three basic interceptors. These interceptors include the wideband radiometer, the chip-rate detector, and the chip-rate detector with a noise reference. The performance of these systems will be evaluated in the presence of white Gaussian noise and various jammer scenarios. The jammer models consist of both continuous wave and pulsed jammers. Receiver operating characteristic (ROC) curves and bit error rate curves will be produced for the various jamming scenarios. Finally, the LPI quality factor will be evaluated, and its behavior as a function of various jamming parameters will be examined.

1.5 Approach

This thesis evaluates the performance of both the intended receiver and the intercept receiver under various noise and jamming conditions defined in Chapter IV. It then looks at the effects of a digital excision filter (DEF) upon both the receiver operating characteristics of the interceptors and the bit error rate (BER) of the intended receiver. In addition, it evaluates the systems' performance through the use of the quality factors defined in Chapter III. The modulation and interference suppression quality factors are examined as a function of the jammer's offset from the carrier, the jammer's pulse repetition frequency, and the jammer's duty cycle. These quality factors can then be related back to the LPI quality factor to illustrate the effects of the jammer parameters and the filtering upon the achievable communication range and intercept range.

1.6 Materials and Equipment

All system models and simulations were developed using the version 3.0 Signal Processing Worksystem (SPW) simulation software developed by Comdisco Systems, Inc of Foster City, California. The software was run on a Sparc2 Sun Workstation in the Communications/Radar Laboratory, room 225, building 640. In addition, Matlab was used to produce the curves using data obtained from the SPW simulations.

1.7 Thesis Organization

Chapter II of this thesis presents a basic introduction into the concept of Direct Sequence Spread Spectrum (DS-SS) communications. It discusses the theory behind the spreading of a signal, the pseudo-noise (PN) spreading codes used, and the interference suppression benefits of DS systems. Chapter III defines the concept behind Low Probability of Intercept (LPI) communications and presents the quality factors used to evaluate a system's LPI performance. In addition, it introduces the basic theory behind the interceptor models used in this research. Chapter IV provides an introduction to communication system simulation and discusses the systems and simulations used through-out this research. Chapter V discusses the results of the simulations, and Chapter VI summarizes the thesis and provides recommendations for future research.

1-4

II. Spread Spectrum Theory

2.1 Introduction

This chapter provides an introduction to spread spectrum theory, the spreading codes used, and the interference suppression benefits that it provides. It was written through the combined efforts of the author and Capt James Lascody (7).

2.2 Spread Spectrum Communications

In all communications systems, the modulated waveform occupies a frequency bandwidth that is dependent upon the modulation method used and the data being sent. In a spread spectrum system, the transmitted bandwidth of the signal has been "spread" over a larger bandwidth than the original modulated bandwidth (3). This transforms the power spectral density into a more uniform spectrum much like that of noise (2). To qualify as spread spectrum, a system must satisfy the following three conditions (17):

1. The signal occupies a bandwidth much in excess of the minimum bandwidth required by the information.
2. Spreading is accomplished through the use of a code signal independent of the data itself.
3. At the receiver, despreading is accomplished by the correlation of the received signal with a replica of the spreading code used at the transmitter.

Spread spectrum (SS) techniques, due to their anti-jam and low probability of intercept characteristics, were initially developed for use in military guidance and communications systems. These technologies were eventually integrated into areas such as energy density reduction, high-resolution ranging, and multiple access systems (17). Currently, because of their ability to reject undesired interference and their low power spectral densities, SS techniques are being investigated for integration into commercial wireless communications systems and cellular telephony. The three general spread spectrum signaling methods are (3):

1. Modulation of a carrier by a digital code sequence whose bit rate is much higher than the information bandwidth. This is known as direct sequence (DS).

2. Carrier frequency shifting in discrete increments dictated by a code sequence. This is called frequency hopping (FH).

3. Pulsed-FM modulation in which a carrier is swept over a wide band during a given interval.

There are also hybrid SS techniques which incorporate a mixture of the above techniques. In this research, only direct sequence will be addressed.

2.2.1 **Direct Sequence Spread Spectrum.** In direct sequence systems, a pseudo-random code is used to modify the carrier phase prior to transmission of the signal. The code sequence has a much higher rate than the original digital data which expands the bandwidth beyond that of the original information bandwidth (2). After reception of the transmitted signal, the spread spectrum receiver must perform two functions beyond that of a conventional receiver. First, the receiver must learn or reproduce the code used by the modulator. This process is known as code acquisition. The acquired code must then be synchronized with the transmitter code. This process is known collectively as synchronization. Second, the receiver must remove the spreading of the carrier bandwidth to obtain the original message bandwidth (12). This process is known as carrier despreading and is accomplished through multiplication of the received signal with a correlated replica of the original spreading code. This reduces the message signal back to its original bandwidth, while spreading any interference that might be present.

In a typical direct sequence system as shown in Figure 2.1, a data signal $d(t)$ is used to modulate a carrier signal $x(t)$ represented by

$$x(t) = \sqrt{2P} \cos[\omega_o t] \qquad (2.1)$$
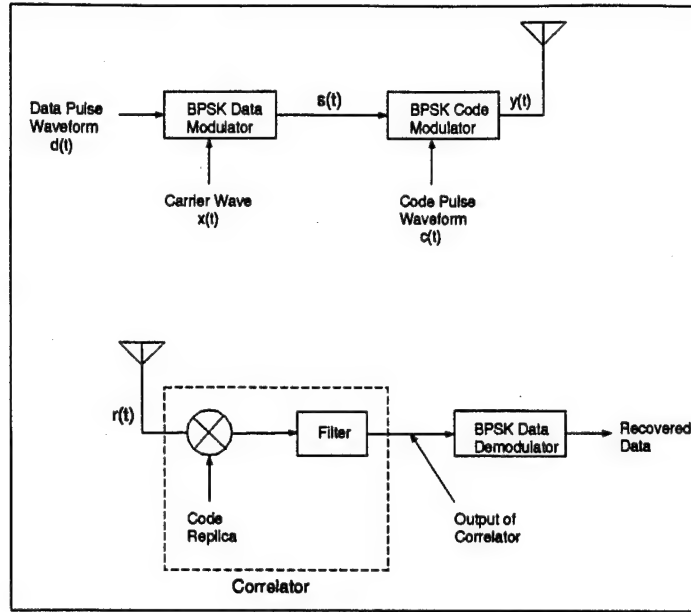
Figure 2.1   Direct Sequence Spread Spectrum Transmitter and Receiver

where ω_o is the radian frequency and P is the carrier power. The modulated waveform is then given by

$$s(t) = \sqrt{2P} \cos \left[\omega_o t + \theta_x(t) \right] \qquad (2.2)$$

where θ_x is the data phase modulation. This signal is then modulated by a spreading code $c(t)$. The resulting waveform is

$$y(t) = \sqrt{2P} \cos \left[\omega_o t + \theta_x(t) + \theta_c(t) \right] \qquad (2.3)$$

where $\theta_c(t)$ is the phase modulation due to the spreading code. For BPSK modulation with antipodal data and spreading signals the expression for $y(t)$ can be reduced to

$$y(t) = \sqrt{2P} \, x(t) \, c(t) \cos \left[\omega_o t \right] \qquad (2.4)$$

2-3

At the receiver, the received signal $r(t)$ is represented by

$$r(t) \;=\; y(t - T_d) \tag{2.5}$$

$$\;=\; A\sqrt{2P}\, d(t - T_d)\, c(t - T_d)\, \cos\left[\omega_o(t - T_d) + \phi\right] \tag{2.6}$$

where A is the system gain parameter, ϕ is a random phase in the range $(0, 2\pi)$, and T_d is the propagation delay which is dependent upon the distance between the transmitter and receiver. This signal is multiplied by the original spreading code that has been delayed by $\hat{T}_d$ which is the receiver estimate of the propagation delay T_d. When the code at the receiver is correlated with the code at the transmitter, $T_d = \hat{T}_d$ and the output of the correlator will be the unspread signal $s(t)$ with a phase difference and a delay. This despread signal is then used as input to a conventional BPSK demodulator (17).

There are two main criteria for measuring the effectiveness of this process. The first criterion, the process gain, compares the input and output signal power to noise power ratios (SNR) and is expressed by:

$$G_p = SNR_{out} - SNR_{in}$$

where SNR_{out} is the output signal power to noise power ratio of a given receiver with an input signal power to noise power ratio SNR_{in} with both quantities in dB's. For example, if SNR_{in} for an SS receiver is -10dB and the SNR_{out} is 15dB, the processing gain would be 25dB. The processing gain can also be expressed by:

$$G_p = \frac{BW_{RF}}{R_{info}}$$

where BW_{RF} is the bandwidth of the transmitted spread spectrum signal, and R_{info} is the data rate of the baseband (unmodulated) data signal (3). For example, if a 1.544Mbps signal is spread to a bandwidth of 20Mhz, the process gain is 12.95 or 11dB (2).

2-4

The second criterion, the jamming margin, measures the system's performance capability in a hostile environment and is expressed by:

$$M_j = G_p - [L_{sys} + SNR_{out}]$$

where L_{sys} is the system implementation loss and SNR_{out} is the minimum receiver output signal power to noise power ratio required to maintain a specified BER with all quantities in dB's (3). The jamming margin is essentially the process gain with an allowance for implementation losses and a minimum acceptable output SNR (2). The jamming margin is the maximum interference power which a system can encounter and still be expected to operate with the desired BER.

2.2.2 **Spreading Codes.** There are two methods that can be employed by a spread spectrum system to obtain the despreading code at the receiver. These are the transmitted reference and the stored reference. In the first of these, the spreading code is simultaneously transmitted with the data. This method is impractical for secure applications and is not commonly used in military applications. The second and more commonly encountered approach is the stored reference. In this method, the code must either be stored or generated by the receiver. When using the transmitted reference, it is possible to use a completely random sequence; however, for the stored reference, a deterministic sequence must be used.

The codes used for this purpose are known as pseudo-random or pseudo-noise (PN) codes. These codes are a class of linear code sequences that despite being deterministic have statistical properties much like that of uniform noise. These codes must satisfy the following properties (17):

1. Balance - Good balance requires that in each period of the sequence, the number of binary ones differs from the number of binary zeros by at most one digit.
2. Run - A run is defined as a sequence of a single type of binary digit(s). The appearance of the alternate digit in a sequence starts a new run. The length of the run is the number of the digits in the run. It is desirable that approximately 2^{-n} of the runs be of length n.

3. Correlation - If the sequence is compared term by term with a cyclic shift of itself, the number of agreements should differ from the number of disagreements by not more than one count.

Codes satisfying these properties will allow for optimum spreading to occur while minimizing the interference between users. The most common method of generating these codes is to use shift
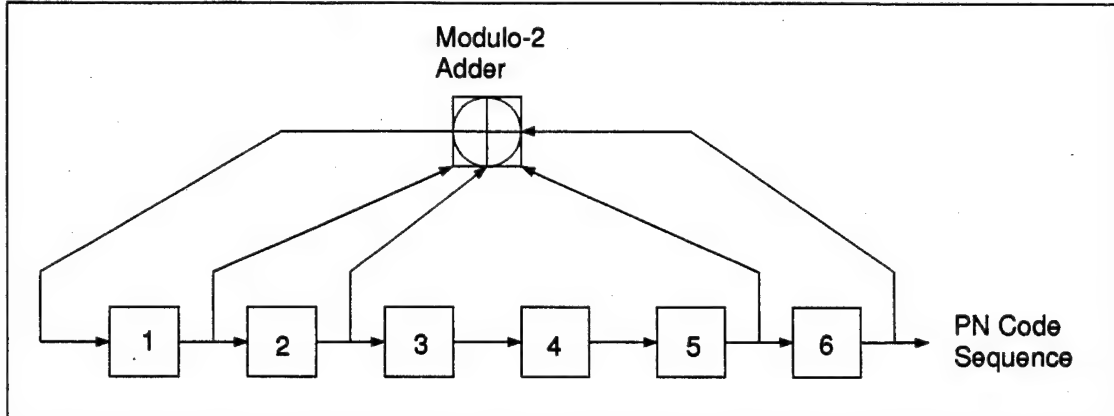
Figure 2.2   Linear Shift Register PN Code Sequence Generator

registers with feedback taps going to a modulo two adder as shown in Figure 2.2. The length of the code, as well its ability to meet the above criteria, is determined by the number of shift registers and the feedback taps used (17) (3). The longest code that can be generated by a shift register of length N is $2^N - 1$.

Effective PN codes have high auto-correlation peaks when they have a zero shift present. These peaks help to minimize false synchronization (2). A typical PN auto-correlation function is shown in Figure 2.3. The auto-correlation function for a code of length p is defined as (17)

$$R_x(\tau) = \frac{1}{p} \begin{bmatrix} number\ of\ agreements\ less\ number\ of \\ disagreements\ in\ a\ comparison\ of\ one\ full \\ period\ of\ the\ sequence\ with\ a\ \tau\ position \\ cyclic\ shift\ of\ the\ sequence \end{bmatrix} \tag{2.7}$$

For example, for the PN code $0\,0\,0\,1\,0\,0\,1\,1\,0\,1\,0\,1\,1\,1\,1$ we can obtain the autocorrelation for $\tau = 1$ by

$$
\begin{array}{l}
0\,0\,0\,1\,0\,0\,1\,1\,0\,1\,0\,1\,1\,1\,1 \\
\underline{1\,0\,0\,0\,1\,0\,0\,1\,1\,0\,1\,0\,1\,1\,1} \\
d\,a\,a\,d\,d\,a\,d\,a\,d\,d\,d\,d\,a\,a\,a
\end{array}
$$

By applying Eqn 2.7, we find that $R_X(1) = (7 - 8)/15 = -1/15$. By repeating this process for all shifts of the sequence, R_x can be plotted as a function of the shift τ similar to Figure 2.3. In addition, codes can be developed which have low cross-correlation with other codes. This low cross-correlation minimizes interference between users and allows for effective Code Division Multiple Access (CDMA) communication.
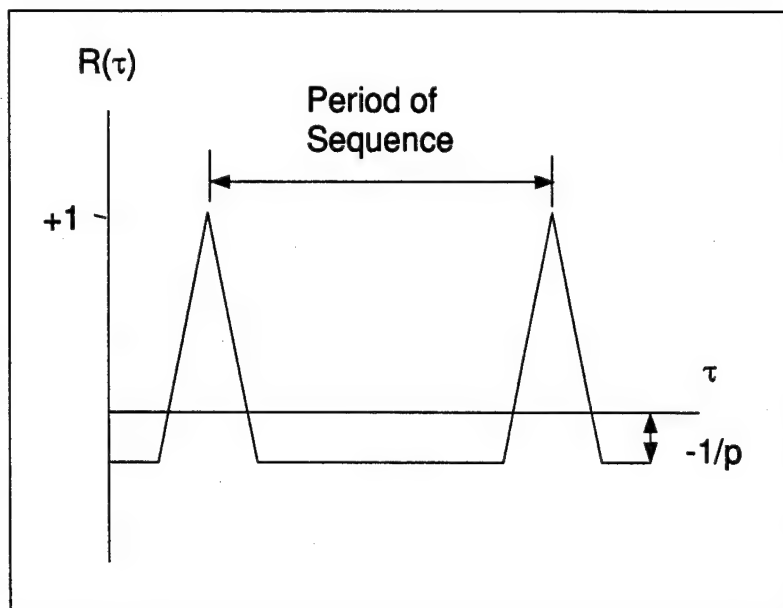
Figure 2.3   Typical PN Auto-Correlation Function

2.3   Interference Suppression in Spread Spectrum

The objective of a jammer is to use a signal source to prevent the intended receiver from obtaining the transmitted data. This can be done through the following types of jamming signals:

- Continuous Wave
- Swept Tone
- Broadband
- Narrowband
- Pulsed Tone

When a jammer is used against a narrow-band signal, the most common jamming method is to produce a high power tone centered at the carrier frequency of the narrow-band signal. When a jammer encounters a spread spectrum signal, it must decide whether to concentrate a high power signal over a relatively narrow portion of the signal, as shown in Figure 2.4, or to spread its power over a larger bandwidth. Regardless of the technique chosen, the effect of the interference will be decreased during
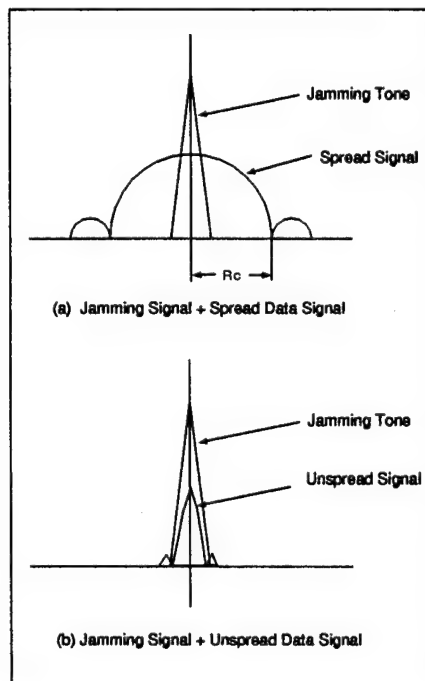
Figure 2.4   Example of Jammer Effects upon Spread and Unspread Signals

the despreading process. When the received signal is multiplied by the spreading code, the jamming signal will be spread in the same manner as the data signal was spread before transmission. Thus, the jammer signal will have a lower power density over a given bandwidth and will be less effective.

In order to obtain analytical insight into the effect of spread spectrum upon jamming signals (8), consider a single tone jammer represented by

$$j(t) = \sqrt{2P_j} \, \cos{(\omega_c t + \theta)} \tag{2.8}$$

where P_j is the jammer power, and we are assuming that the jammer power is much greater than the noise power such that $P_j + P_N \approx P_j$. The received signal can then be written as

$$r(t) = \sqrt{2P_s} \, d(t) \, c(t) \, \cos{(\omega_c t)} + \sqrt{2P_j} \, \cos{(\omega_c t + \theta)} \tag{2.9}$$

where P_s is the signal power. After $r(t)$ is multiplied by the replica of the code sequence and is carrier demodulated, the resultant signal can be written as

$$
\begin{aligned}
r(t) = {} & \sqrt{P_s} \, d(t) \, [1 + \cos{(2\omega_c t)}] + \sqrt{P_j} \, c(t) \, [1 + \cos{(2\omega_c t)}] \cos{(\theta)} \\
& - \sqrt{P_s P_j} \, \sin{(2\omega_c t)} \sin{(\theta)}
\end{aligned}
\tag{2.10}
$$

The signal is then filtered to remove double frequency terms and the output of the demodulator is

$$r_o(t) = P_s \, d(t) + \sqrt{P_s P_j} \, c(t) \, \cos{(\theta)} \tag{2.11}$$

From Eqn 2.11, $r_o(t)$ consists of the desired information signal, $d(t)$, plus an interference term. The PSD of this interference term can be expressed as (18)

$$S_{jj} = \frac{P_j \, \overline{\cos^2{\theta}}}{2R_c} \, sinc^2\left(\frac{f}{R_c}\right) \tag{2.12}$$

2-9

where R_c is the code chip rate. After this is integrated over the period T_b, which has an effect equivalent to a lowpass filter with a cutoff frequency of R_b, we get approximately

$$S_{jj} = \frac{P_j \overline{\cos^2 \theta}}{2R_c}$$ (2.13)

Then, letting $N_o \cong S_{jj}$ in the equation for P_e for coherent BPSK, we get

$$P_e = Q\left[\sqrt{\frac{2E_b}{N_o}}\right]$$ (2.14)

$$= Q\left[\sqrt{\frac{4R_c E_b}{P_j \overline{\cos^2 \theta}}}\right]$$ (2.15)

Then , making use of the expressions $E_b = P_s T_b$ and $T_b = \frac{1}{R_b}$ along with the fact that $\overline{\cos^2 \theta} = \frac{1}{2}$ for the range $[0, 2\pi]$ we can write

$$P_e = Q\left[\sqrt{\frac{4P_s G_p}{P_j}}\right]$$ (2.16)

where $G_p = \frac{2R_c}{R_b}$.

Through the same type of analysis, it can be shown that a worse case approximation for multiple narrowband jammers is given by

$$P_e = Q\left[\sqrt{\frac{4P_s G_p}{\sum_{i=1}^{n} P_{j,i}}}\right]$$ (2.17)

This approximation assumes that the jammers are uncorrelated, and that the difference between the carrier frequency and the jammer frequency is small compared to the carrier frequency itself. For the simulations in this thesis, the last criteria was met by keeping the carrier frequency much smaller than the simulation bandwidth.

III. LPI Communications and Signal Interception Techniques

3.1 Introduction

This Chapter provides an overview of the objectives of LPI communications and the quality factors used to quantify LPI performance. In addition, it introduces the interception techniques and interceptor models used in this research effort.

3.2 LPI Communications

The objective of LPI communications is to limit the range at which a signal can be intercepted by an unintended receiver without a reduction in the communication range of the intended receivers. This objective is illustrated in Figure 3.1. In this figure, the transmitter (T) transmits a signal to the
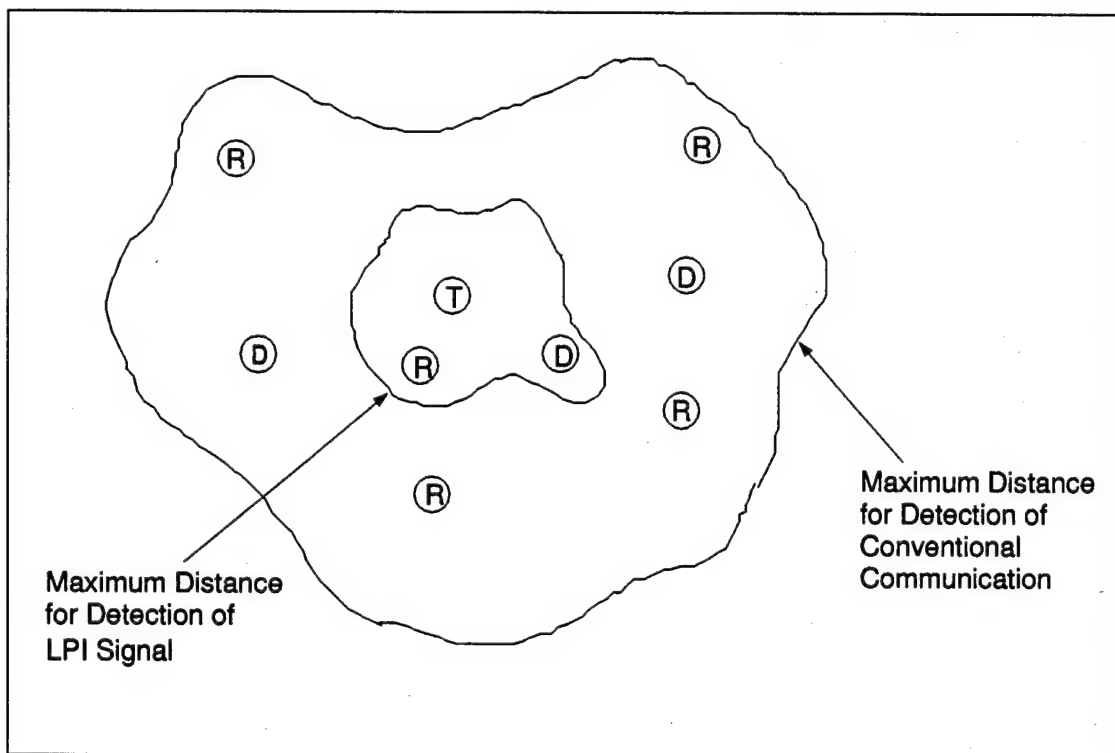
Figure 3.1 Illustration of LPI Concept

intended receivers (R) while the intercept receivers (D) attempt to also detect the signal. If conventional

waveforms are used, the intercept receivers may be able to detect the signal at large distances from the transmitter. When LPI waveforms are used, the intended receivers are able to receive the signal at large distances, while the interceptors must move much closer to the transmitter.

There are numerous techniques that can be used to achieve LPI communications. Among these are high-gain directional antennas, interactive RF power control, and custom waveform design. One example of a waveform designed for this purpose is direct sequence spread spectrum. By spreading the message signal, the RF power density of the signal is reduced and thus, the LPI characteristics are improved. Along with the LPI benefits, the DS-SS also produces interference suppression benefits as discussed previously.

In a typical communication scenario shown in Figure 3.2, the benefits of using an SS signal are further highlighted. In this situation, multiple jammers are attempting to disrupt the signal and deny
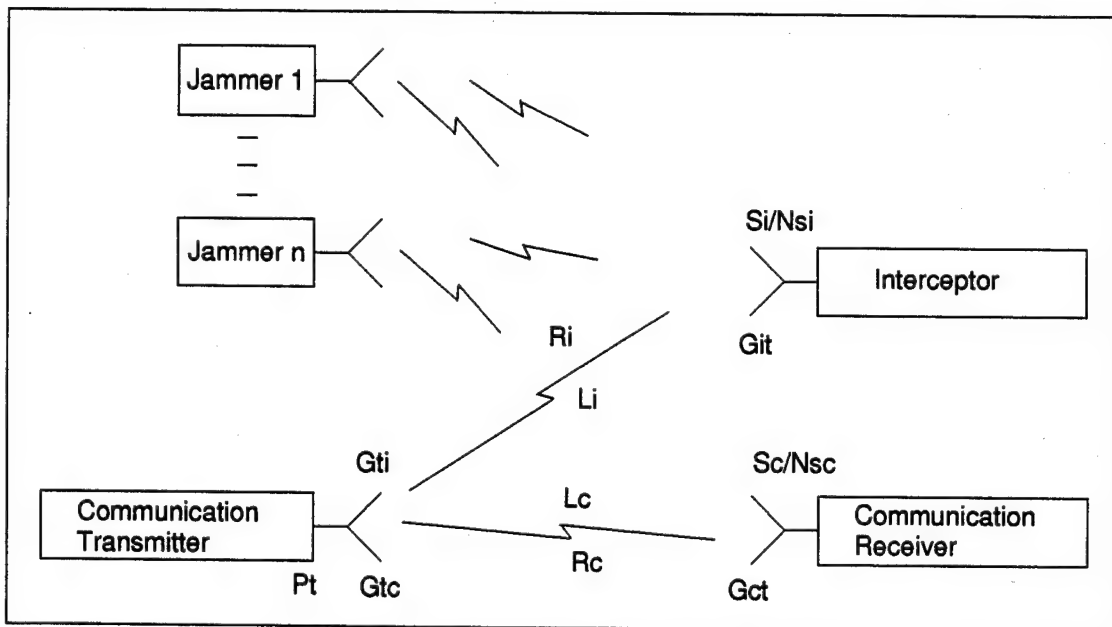
Figure 3.2   Typical Communication Scenario in a Hostile Environment

the intended receiver the information it desires. At the same time, the intercept receiver attempts to detect the signal. Once again, the SS benefits help to prevent the intercept receiver from detecting the signal while reducing the detrimental effects of the jammers. In order to illustrate these effects, and

to further explore the LPI concept, link analysis can be used to analyze Figure 3.2. The results of the link analysis are various quality factors which can be used to characterize the performance of a given system. The complete link analysis and all parameter definitions are contained in Appendix A. The bottom line results that will be used in the remainder of this research are the communication range R_c and the intercept range R_i. The communication range, which is the maximum range at which a receiver can still maintain a required bit error rate, can be expressed as

$$R_c = \sqrt{\frac{P_t G_{tc} G_{ct}}{L_c N_{sc}} \left(\frac{\lambda}{4\pi}\right)^2 \frac{1}{S_c/N_{sc}}} \tag{3.1}$$

The intercept range, which is the maximum range at which an interceptor can maintain required detection and false alarm rates, can be expressed as

$$R_i = \sqrt{\frac{P_t G_{ti} G_{it}}{L_i N_{si}} \left(\frac{\lambda}{4\pi}\right)^2 \frac{1}{S_i/N_{si}}} \tag{3.2}$$

These two expressions can then be used to obtain the LPI equation which is

$$\left(\frac{R_c}{R_i}\right)^2 = \frac{G_{ct} G_{tc}}{G_{it} G_{ti}} \frac{L_i}{L_c} \frac{N_{si}}{N_{sc}} \frac{S_i/N_{si}}{S_c/N_{sc}} \tag{3.3}$$

The main objective is to maximize this equation. This will provide for the largest possible R_c while forcing the interceptors to move closer to the transmitter.

There are numerous possible ways to improve LPI performance. As mentioned earlier, directional antennas, coding, and different modulation schemes will all affect the ratio of R_c/R_i. Quality factors are used as a means of quantifying these trade-offs and allowing the designer some degree of flexibility in meeting the LPI needs of the user. The first quality factor, the *LPI Quality Factor*, is defined to be

$$Q_{LPI} = 20 \log \left(\frac{R_c}{R_i}\right) \tag{3.4}$$

This can be broken into a sum of additional quality factors and is expressed as

$$Q_{LPI} = Q_{ANT} + Q_{ATM} + Q_{IS} + Q_{MOD} \qquad (3.5)$$

where

- Q_{ANT} is the antenna quality factor
- Q_{ATM} is the atmospheric quality factor
- Q_{IS} is the interference suppression quality factor
- Q_{MOD} is the modulation quality factor

These quality factors are defined and discussed in Appendix A. The only factors that are of concern in this research are Q_{MOD} and Q_{IS}. The modulation quality factor is dependent only upon the type of modulation and detection that is employed and thus eliminates any scenario dependent variables. It is defined to be

$$Q_{MOD} = 10 \log \left(\frac{S_i/N_{si}}{S_c/N_{sc}} \right) \qquad (3.6)$$

where S_i/N_{si} is the signal power to noise-plus-interference PSD ratio required by the interceptor to maintain a given probability of false alarm and probability of detection, and S_c/N_{sc} is the signal power to noise-plus-interference PSD ratio required by the communication receiver to maintain a given BER. This can be further expressed as

$$Q_{MOD} = \frac{\zeta_i(P_D, P_F, T, W)}{\zeta_c(P_e)R_b} \qquad (3.7)$$

where $\zeta_i(P_D, P_F, T, W)$ is an expression for the input signal power to noise-plus-interference PSD ratio required by a given intercept receiver to maintain a desired probability of detection, P_D, and a desired probability of false alarm, P_F, given that the receiver has a bandwidth of W and an integration period of T. Similarly, $\zeta_c(P_e)$ is an expression for the input signal power to noise-plus-interference PSD ratio required by a given communication receiver to maintain a desired probability of error,

P_e, for a specific modulation scheme, and R_b is the bit rate of the communication system. Both $\zeta_i(P_D, P_F, T, W)$ and $\zeta_c(P_e)$ are dependent upon the specific modulation and detection scheme being employed. $\zeta_i(P_D, P_F, T, W)$ is developed for the radiometer and chip rate detector in future sections, and $\zeta_c(P_e)$ is given for a BPSK system in the next paragraph.

For a BPSK modulated signal, we can use the expression for P_e to find $\zeta_c(P_e)$. It is well known that P_e for BPSK is given by

$$P_e = Q\left[\sqrt{\frac{2E_b}{N_{sc}}}\right] \tag{3.8}$$

Solving this for E_b/N_{sc} we get

$$\frac{E_b}{N_{sc}} = \frac{[Q^{-1}(P_e)]^2}{2} \tag{3.9}$$

This is a simple form expression, and values can be easily obtained from an inverse Q table or a computer program. The value obtained for E_b/N_{sc} can then be used to find $\zeta_c(P_e)$. However, not all modulation schemes can be represented by such a simple expression. For example, to find the $\zeta_c(P_e)$ for a 32-ary cyclic code shift keying modulation scheme as employed by the Joint Tactical Information Distribution System (JTIDS), it would be necessary to solve the following expression for the input signal energy to noise PSD ratio

$$P_e = \frac{1}{62}\sum_{n=1}^{32}\binom{32}{n}(-1)^n \exp\left[-5\frac{E_b}{N_{sc}}\left(\frac{n-1}{n}\right)\right] \tag{3.10}$$

Given a desired P_e, Eqn 3.10 must be solved recursively for E_b/N_{sc}. Thus, it is often more convenient to use the bit error rate curves available for specific modulation schemes.

In addition to Q_{MOD}, the interference suppression quality factor must also be considered due to the use of the excision filter. Because of the complexity of the expression for Q_{IS} (shown in

Appendix A), it is beyond the scope of this thesis to derive an actual expression quantifying the effects of the DEF. Thus, the modulation and interference suppression quality factors will be combined into a composite quality factor, Q_{COMP}, which will be evaluated empirically. If we assume that the noise and interference environments in which the interceptors and communication receiver operate are identical, we can express Q_{COMP} as

$$Q_{COMP} = 10log\left(\frac{S_i}{S_c}\right) \tag{3.11}$$

where S_i is the transmitted signal power required by the intercept receiver to maintain desired false alarm and detection rates, and S_c is the transmitted signal power required by the communication receiver to maintain a desired P_e. To obtain values for Q_{COMP}, the minimum acceptable P_d and P_f and the maximum acceptable P_e will be defined. Simulations will then be run to find the minimum transmitted signal powers at which these values occur. These values can then be used in the above expression to find Q_{COMP}.

3.3 Interception Techniques

The objective of an intercept receiver is to make a decision concerning the presence of a signal. It does this through statistical decision theory and hypothesis testing. The intercept receiver generates a test statistic which is then compared to a decision threshold V_T. If the test statistic is below the threshold, the detector chooses hypothesis H_0 (no signal). If the test statistic exceeds the threshold, hypothesis H_1 (signal present) is chosen. A false alarm occurs when hypothesis H_1 is chosen when in fact no signal is present. A miss occurs when hypothesis H_0 is chosen when a signal is actually present. Finally, a detection occurs when hypothesis H_1 is chosen when there is actually a signal present. The probability of a false alarm is defined to be

$$P_F = \int_{V_T}^{\infty} f_{V|H_0}\left(v \mid H_0\right) dv \tag{3.12}$$

and the probability of detection is

$$P_D = \int_{-\infty}^{V_T} f_{V|H_1}\left(v \mid H_1\right) dv \tag{3.13}$$

where $f_{V|H_0}$ and $f_{V|H_1}$ are the conditional probability density functions for the two hypotheses. The probability of a miss is simply $P_M = 1 - P_D$.

In this thesis, two types of detectors are used. These are the wideband radiometer and the chip rate detector. In addition two variations of the chip rate detector are used. These detectors are discussed in greater detail in the next two sections.

3.3.1 **Wideband Radiometer.** The radiometer is the simplest form of intercept receiver and is shown in Figure 3.3. It forms a test statistic by estimating the energy that is received in a bandwidth W over an observation time T. If the test statistic is above a given threshold, the interceptor assumes a signal is present. Otherwise, it assumes there is no signal being transmitted. The operation of the
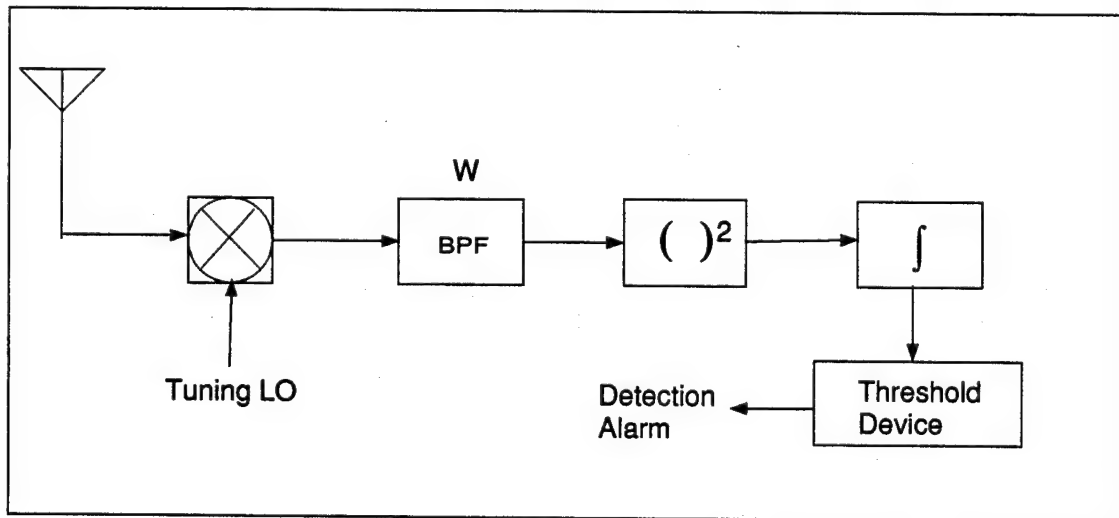
Figure 3.3   Block Diagram of a Wideband Radiometer

radiometer can be observed through the following analysis. If we assume that for some input signal to

the radiometer, the output of the BPF is $x(t)$ and is expressed by

$$x(t) = s(t) + n(t) \tag{3.14}$$

where $s(t)$ is the signal of interest and $n(t)$ is bandpass filtered additive white Gaussian noise (AWGN), we can write the output of the integrator as

$$
\begin{align}
V(t) &= \int_0^T x^2(t)dt \tag{3.15} \\
&= \int_0^T [s(t) + n(t)]^2 \, dt \tag{3.16} \\
&= \int_0^T \left[s^2(t) + 2s(t)n(t) + n^2(t) \right] dt \tag{3.17}
\end{align}
$$

We can then take the expected value of $V(t)$ and, assuming that $n(t)$ is a zero-mean process with two-sided power spectral density of $\frac{N_{oi}}{2}$, we obtain

$$
\begin{align}
E[V] &= \int_0^T E\left[s^2(t)\right] dt + \int_0^T E\left[n^2(t)\right] dt \tag{3.18} \\
&= E_s + N_{oi}TW \tag{3.19}
\end{align}
$$

where E_s is the signal energy. If we then normalize this expression by $\frac{2}{N_{oi}}$, $E[V]$ is given by

$$E[V] = \frac{2E_s}{N_{oi}} + 2TW \tag{3.20}$$

Because of the squaring operation V will take on a Chi-Square distribution that has $2TW$ degrees of freedom for a noise only input. When the input contains both a signal and noise, it will take on a non-centrality parameter of $2E_s/N_{oi}$ (19).

In order to derive the expression for $\zeta_i(P_D, P_F, T, W)$ for use in the modulation quality factor given by Eqn 3.7, we must find an expression for the required intercept signal power to noise PSD

ratio. From (12), we find that for a wideband radiometer

$$(SNR)_{out} = \frac{S_i^2 TW}{N_{oi}^2 + 2S_i N_{oi}} \tag{3.21}$$

$$= \frac{S_i^2 TW}{N_{oi}^2 (1 + 2S_i/N_{oi})} \tag{3.22}$$

$$= \frac{(SNR)_{in}^2 TW}{1 + 2(SNR)_{in}} \tag{3.23}$$

$$\tag{3.24}$$

where S_i is the average signal power at the interceptor and N_{oi} is the power spectral density of the noise at the interceptor. For a low input signal power to noise PSD ratio where $N_{oi}^2 \gg 2S_i N_{oi}$, we can reduce this to

$$(SNR)_{out} = \frac{S_i^2 TW}{N_{oi}^2} \tag{3.25}$$

$$= (SNR)_{in}^2 TW \tag{3.26}$$

Solving this for $(SNR)_{in}$ we obtain

$$(SNR)_{in} = \sqrt{\frac{(SNR)_{out}}{TW}} = \frac{S_i}{N_{oi}W} \tag{3.27}$$

We can then refer to $(SNR)_{out}$ as the detectability factor d^2 which can be expressed in terms of P_F and P_D as

$$d^2 = \left[Q^{-1}(P_F) - Q^{-1}(P_D) \right]^2 \tag{3.28}$$

Thus, the input signal power to noise PSD ratio required by the radiometer to obtain a desired P_F and P_D can be expressed as

$$\frac{S_i}{N_{oi}} = (SNR)_{req} = \sqrt{\frac{(SNR)_{out}W}{T}} = d\sqrt{\frac{W}{T}} \tag{3.29}$$

$$= \zeta_i(P_D, P_F, T, W) \tag{3.30}$$

This detection model is known as Edell's model (10) and can be used to calculate the modulation quality factor for the wideband radiometer. It is reasonably accurate (within 0.5dB) for large time bandwidth products where $TW \geq 100$. Finally, we can add interference by replacing N_{oi} with $N_{si} = N_{oi} + N_{ji}$ (see Appendix A).

3.3.2 **Chip Rate Detector.** The chip rate detector, shown in Figure 3.4, relies upon the fact that when certain non-linear operations are applied to a PSK signal discrete spectral components will appear (6). The non-linear operation that will be considered in this thesis is the delay and multiply device. This device produces spectral lines at multiples of the bit frequency for non-spread signals and at multiples of the chip rate for DS-SS signals. It produces these spectral lines by delaying the signal by one half of its bit or chip period and multiplying this by the un-delayed signal. This produces a change in the sign of multiplication whenever the code stream changes state. This forms a partial PN code clock which can be detected with a band-pass filter placed at the bit or chip frequency. This is due to the fact that the delay and multiply device exploits the periodicity of the phase terms that are present in PSK modulation (15).

To derive the expression for $\zeta_i(P_D, P_F, T, W)$ for the chip rate detector, we will follow the same method used for the radiometer. The first step is to obtain the signal to noise ratio after the second band-pass filter of Figure 3.4. From (15), we find that this can be expressed as

$$(SNR)_1 = \frac{1}{4}(SNR)_{in}\frac{B_1}{B_2} \tag{3.31}$$

3-10
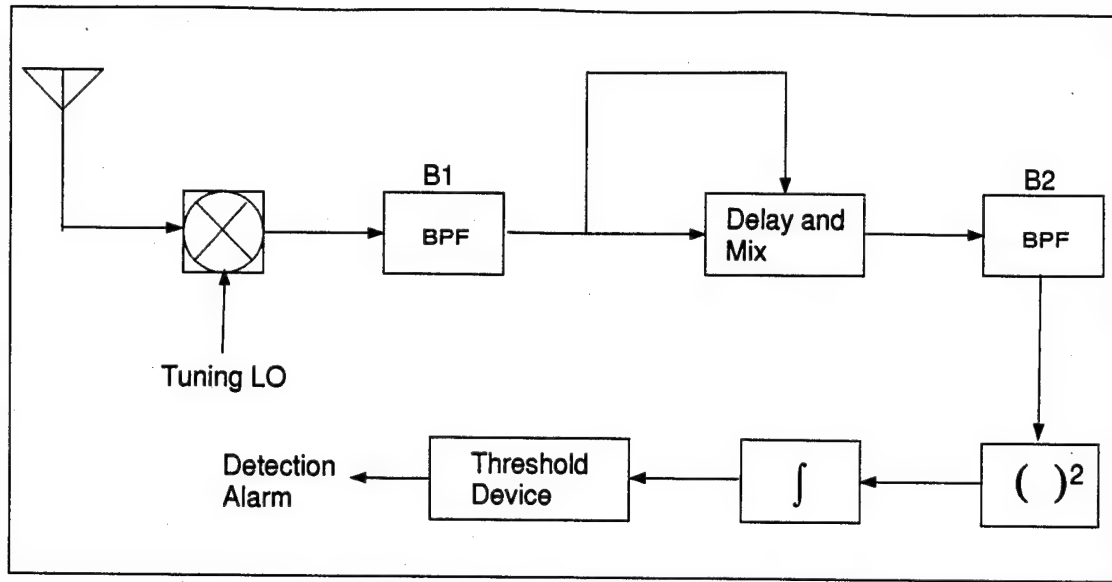
Figure 3.4   Block Diagram of a Chip Rate Detector

The remainder of the chip rate detector after the second band-pass filter is identical to the radiometer. Thus, using the expression derived earlier

$$(SNR)_{out} = (SNR)_1^2 TB_2 \tag{3.32}$$

$$= \frac{1}{16}(SNR)_{in}^4 \frac{B_1^2 T}{B_2} \tag{3.33}$$

Solving this for $(SNR)_{in}$, we get

$$(SNR)_{in} = \left[16(SNR)_{out}\frac{B_2}{B_1^2 T}\right]^{1/4} \tag{3.34}$$

$$= \frac{S_i}{N_{oi} B_1} \tag{3.35}$$

Thus, the signal power to noise PSD ratio required by the chip rate detector can be expressed as

$$\frac{S_i}{N_{oi}} = \left[16(SNR)_{out}\frac{B_1^2 B_2}{T}\right]^{1/4} \tag{3.36}$$

3-11

$$= \left[16d^2 \frac{B_1^2 B_2}{T} \right]^{1/4} \tag{3.37}$$

where d^2 is the detectability factor previously defined as $\left[Q^{-1}(P_F) - Q^{-1}(P_D) \right]^2$. As was stated in the previous section, we can add interference to this expression by replacing N_{oi} with $N_{si} = N_{oi} + N_{ji}$. In the remainder of this thesis, it will be assumed that the communication receiver and intercept receivers are operating in identical noise and interference environments. Therefore, $N_{oi} = N_{oc} = N_o$ will be used for simplicity.

The next interceptor that is used in this research is a modified version of the chip rate detector just described. This interceptor block diagram was obtained from (9). In this interceptor, shown in Figure 3.5, a noise reference has been added in an attempt to reduce the effects of narrow-band interference. When a narrow-band tone is added to a signal, the chip rate detector produces cross-products during the squaring operation. These cross-products produce spectral spikes which can be
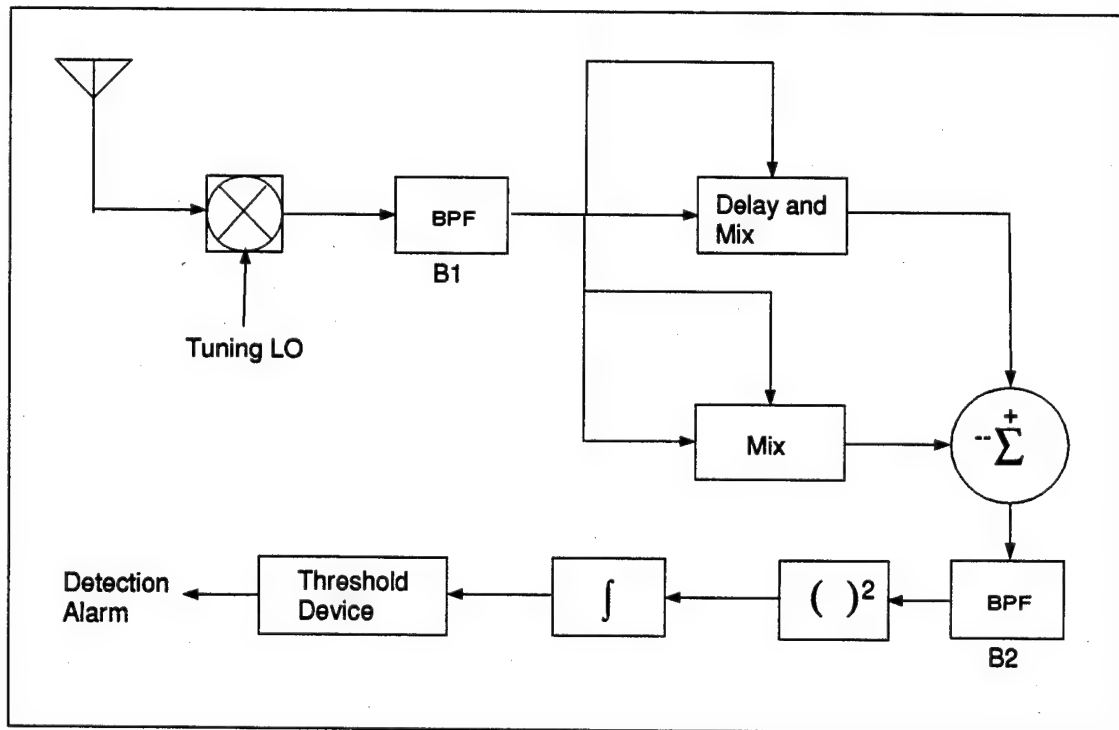
Figure 3.5   Chip Rate Detector with Noise Reference

confused with the spikes present at the chip frequencies. This raises the probability of false alarm and reduces the detector's effectiveness.

The noise reference is simply a second squaring operation with no delay. This produces the same cross-products as the delay and squaring; however, it does not produce the spectral lines at the chip frequencies. The output of the delay and multiply channel and the noise reference channel are then subtracted. This is then passed onto a radiometer which detects the desired chip line.

IV. Simulation of Communication Systems and SPW Blocks

4.1 Introduction

This chapter provides an overview of the theory behind the simulation of communication systems. It then introduces the SPW simulation blocks and system models used during this research. Sections 4.2 through 4.3.2 were written through the combined efforts of Capt James Lascody (7) and the author.

4.2 Simulation Background

Over the past decade, the role of simulation has changed drastically. Simulation was previously used to simply check system functionality and evaluate performance characteristics. Now, simulation is fully integrated into the design process, making it easier to move from a top level design toward the implementation of the system (16). Engineers typically have access to extremely powerful computers, which has helped to drive the interest in the simulation area. Whether one is performing a mathematical calculation or running a computer simulation, the basis for each starts with a system model. This model typically takes the form of a block diagram that shows the subsystem connections (16). All blocks in the system are defined by a signal processing algorithm which describes the relationship between the input and the output. Although calculations and simulation strive to determine performance parameters of the system, simulations differ from calculations in that the simulations estimate the results whereas the other is a direct calculation. Thus, the result for a calculation is usually a number, but the simulation result is a random variable. Shanmugan is quick to point out that simulation should never be a complete substitute for mathematical analysis. Instead, simulation and analysis should be used together in the development of the system.

4.3 Signal Representation

Two major problems are present when simulation is used to simulate a communication system. First, analog waveforms of the actual system must be represented using discrete-time samples. So, the waveforms must be sampled in a way that not only reduces the effects of aliasing, but also does not oversample the waveform. Oversampling the waveform will cause the simulation to have a large runtime. Second, the analog filters of the actual system must be mapped correctly to digital filters. For a given communication system, lowpass and bandpass signals are present. The lowpass signals are the information bearing waveforms and the bandpass signals are the modulated waveforms, such as the transmitter output and receiver input. As stated earlier, these waveforms must be sampled to obtain the discrete time sequences. The sampling theorem states:

> A bandlimited signal $x(t)$ with $X(f) = 0$ for $|f| \geq f_M$ is uniquely determined by its sample values $x(nT_s)$ at a sequence of equidistant points $t = nT_s$ if $f_s > 2f_M$, where $f_s = 1/T_s$. The sampling frequency $f_s = 2f_M$ is known as the Nyquist rate (1).

A number of other factors influence the choice of sampling frequency and are as follows:

1. Aliasing errors
2. Frequency warping in digital filters
3. Nonlinearities
4. Computational constraints

The computational constraints can be the most demanding factor in the choice of sampling frequency. This is even more true for direct sequence spread spectrum systems with an extremely fast chipping sequence. Thus, the goal is to minimize the sampling rate as much as possible. To do this, we wish to use signals with low pass spectra (16). Low pass signals are then sampled directly with the appropriate sampling frequency. Bandpass signals also can be directly sampled but the number of samples can be greatly reduced. By using the complex envelope, bandpass signals and modulated signals can be simulated as low pass signals. A modulated signal with carrier frequency f_c can be written as follows:

$$x(t) = R(t)cos[2\pi f_c t + \phi(t)] \tag{4.1}$$

where $R(t)$ represents the real envelope of $x(t)$ and $\phi(t)$ represents the phase deviation (16). Using phasors, this equation can be written as:

$$x(t) = Re\left[R(t)e^{j2\pi f_c t}e^{j\phi(t)}\right] \tag{4.2}$$

The complex envelope of this signal is then given as:

$$\tilde{x}(t) = R(t)e^{j\phi(t)} \tag{4.3}$$

The complex envelope of the real signal $x(t)$ is slowly varying with respect to the carrier frequency. By using the complex envelope, the sampling frequency can be significantly lower since the bandwidth of the lowpass signal is usually much smaller than the carrier frequency. This yields a smaller number of samples for a specific time period of $x(t)$. The complex envelope can then be expressed in rectangular form as

$$\tilde{x}(t) = x_i(t) + jx_q(t) \tag{4.4}$$

where $x_i(t)$ and $x_q(t)$ are the in-phase (real) and quadrature (imaginary) components, respectively (16).

4.4 Evaluation Techniques

As stated previously, the goal of the simulation is to estimate the performance characteristics of the communication system. The single most important feature of the digital communication system is the bit error rate (BER) (1) (16). For our simulations the BER describes the fractional number of errors in a transmitted sequence (1). Jeruchim and others describe and examine five simulation based approaches for estimating BER.

1. Monte Carlo (MC) simulation
2. Importance Sampling

3. Extreme-value theory

4. Tail extrapolation

5. Quasi-analytical

The simulations in this research used the first and fifth techniques, which are described in the following sections.

4.4.1 **Monte Carlo Simulation.** Monte Carlo simulation is the brute force method for estimating BER. The simulation processes a certain number of symbols and the BER is calculated by dividing the number of errors by the total number of symbols. Generally, this will give a sample BER that is consistent and unbiased (16). One of the nuances associated with this technique involves synchronization. To compare the original data to the demodulated data, the processing delay must be known so that the original and demodulated streams are aligned in time. Otherwise, excessive errors will result not because of noise, but because the data sequences are not aligned. Advantages of this technique include the fact that it works for any kind of system and that the signals generated by the simulation are almost identical to the actual signals in the system. The biggest detractor, especially when examining low bit rate DS SS systems, is the computational time. As the runtime approaches infinity, the BER estimate becomes more consistent and unbiased (16). A rule of thumb for determining the number of iterations is to set the number of iterations so that 50 to 100 errors are counted. For low data rate, high processing gain DS SS systems, this results in a very long runtime.

4.4.2 **Quasi-analytical Estimation.** Quasi-analytical, or semi-analytical, estimation can reduce the simulation time drastically, but places more burden on the analyst (16). This technique combines simulation and analysis. To invoke this method, a noiseless waveform is generated at the receiver and then, by assuming the noise is additive and has a known pdf, the BER is calculated (1). It is obvious that the time reduction is there since we do not have to wait for errors to occur. For low bit rate, high processing gain DS SS systems, this technique allows allows the user to conduct

many studies in comparison to the MC method. Jeruchim and others point out that the semi-analytic technique should be implemented in any simulation for the following reasons:

1. In linear channels, it can provide the correct answer rapidly.
2. It can be used as a check for the MC simulations under the same conditions.
3. The technique is easy to implement.

The only "catch" or disadvantage to this technique is that the BER must be calculable conditioned on the transmitted data pattern (16). Shanmugan also clarifies this by stating that to be able to use the semi-analytic estimation technique, the noise must be stationary, additive and Gaussian; the noise and data must be uncorrelated; and there must be no nonlinearities after the insertion of the noise (16). For the simulations in this research, these conditions were met. The semi-analytic technique yielded BERs extremely close to those of the MC technique.

4.5 SPW Simulation

The simulation tool used in this research was Comdisco's Signal Processing Worksystem (SPW). This software package allows the user to build a block diagram of a system and then simulate the system to obtain signal waveforms. These waveforms can then be used in the evaluation of various system parameters such as bit error rate evaluations, eye diagrams, scatter plots, and numerous others. The information obtained in these evaluations can then be used to debug and refine the system being developed. SPW allows the user to build complex systems from the system or function blocks already available in pre-developed libraries. In addition, the user has the ability to develop custom blocks.

The SPW software is centered around the Block Diagram Editor (BDE). This is a tool which allows the individual components of the system to be arranged and interconnected. The blocks are arranged in a hierarchical system which allows complex components to be replaced by simple representative blocks. The user can build and save complex systems for use in future designs. In addition, the user can develop custom blocks through the use of the SPW Prepare Block tool. This produces a C program template to which the user can add his own custom functions. By compiling

4-5

the program and linking it to a custom developed symbol, the user has the ability to implement any function which is not available in the standard SPW block libraries. This capability makes SPW an extremely powerful tool and allows the user to model almost any system.

In addition to the BDE, the SPW software contains a Signal Calculator which gives the user the ability to manipulate the signals obtained through the simulations. The Signal Calculator is capable of handling both real and complex signals in addition to real and complex vectors. This tool provides for the execution of many signal processing tools such as FFT's, cross-correlations, auto-correlations, power spectral densities, as well as the bit error rate evaluation, eye diagrams, and scatter plots previously mentioned. Finally, the Signal Calculator allows the user to produce custom signals for use as input to other simulations.

4.6 SPW Simulation Blocks

The overall block diagram used in this research is shown in Figure 4.1. It consists of a random data source, DS-BPSK transmitter and receiver, a transmission channel, a jamming source, and an interceptor. In addition, it includes parameters used to adjust simulation constraints such as the sampling frequency, processing gain, bit rate, jammer power, etc. In this section, the overall block diagram will be discussed and then each individual component will be discussed.

The first component of the system in Figure 4.1 is the random data source. This block produces a random binary data stream which is used as the input to the DS-BPSK transmitter. After reaching the transmitter, this data is BPSK modulated and then spread by a PN sequence. This spread data is then transmitted into the channel where AWGN and jammer signals are added to the waveform. The channel output is then sent to the excision filter which processes the waveform in order to reduce the effects of any jammer signals present. In addition, the channel output is also sent to the interceptor, either the radiometer or chip rate detectors. After the filtering process is complete, the output of the
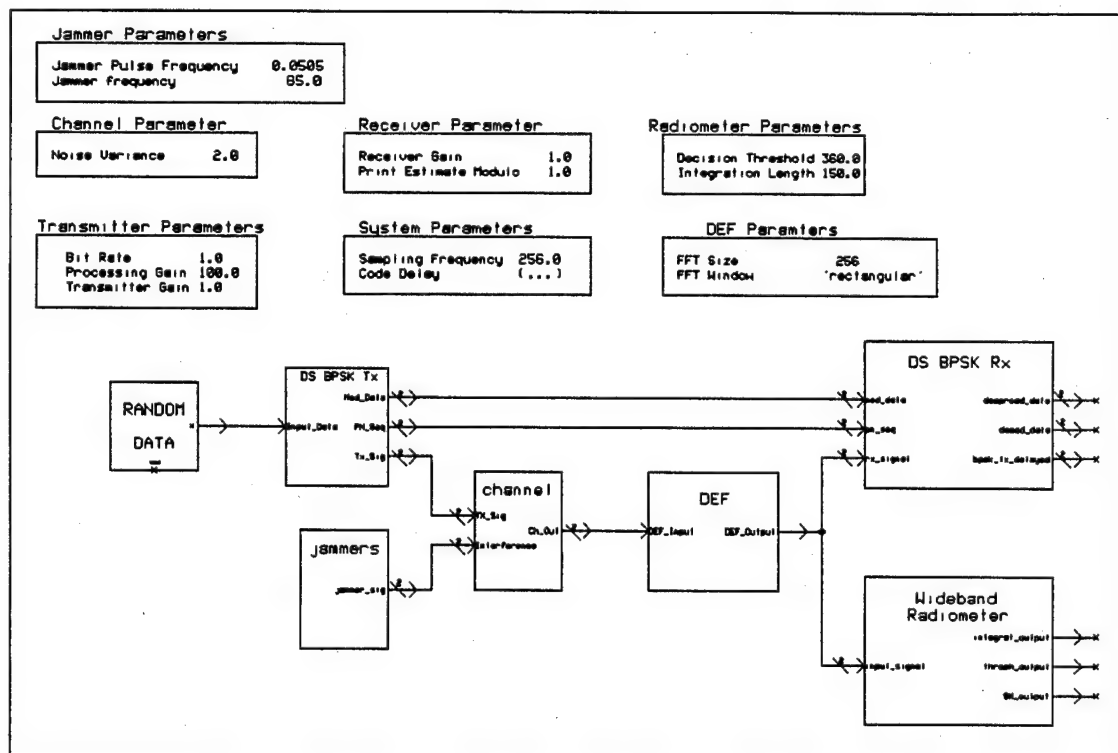
Figure 4.1   Overall System Block Diagram

filter is sent to the DS-BPSK receiver where the signal is despread and demodulated. The parameters which are required for the simulations are as follows:

- Sampling Frequency - the number of samples taken per data bit
- Code Delay - the delay introduced by the channel and despreader
- Bit Rate - the data rate of the random data block
- Processing Gain - the number of PN chips per data bit
- Transmitter Gain - the signal amplification induced prior to transmission
- Noise Variance - controls the noise power in the channel
- Receiver Gain - the signal amplification induced upon reception
- Print Estimate Modulo - the rate at which BER estimates are produced
- Jammer Pulse Frequency - the pulse repetition frequency of the jammer
- Jammer Frequency - the center frequency of the jammer tone
- Decision Threshold - the threshold of the interceptor
- Integration Length - the integration period of the interceptor
- FFT Size - the size of the FFT used by the DEF
- FFT Window - the type of window used by the DEF

4.6.1 **BPSK Direct Sequence Transmitter and Receiver.** The heart of this system is the DS-BPSK communication system consisting of the transmitter, the receiver, and the channel. The transmitter, shown in Figure 4.2, modulates the input data and then multiplies the modulated signal with a PN code sequence generated by a linear shift register code generator. The rate of the spreading code is controlled by the parameter for the processing gain. In addition to the modulation and spreading, the transmitter has a gain parameter which can be used to adjust the power of the transmitted signal. The transmitter gain required for a given E_b/N_o is expressed by

$$T_{x,gain} = \left[\frac{2 \left(\frac{E_b}{N_o} \right) \sigma^2 R_b}{f_s} \right]^{\frac{1}{2}} \tag{4.5}$$

where σ^2 is the noise variance, R_b is the bit rate, and f_s is the sampling frequency (also known as the simulation bandwidth). After the gain of the signal has been adjusted, the signal is sent to the channel

block. This block, shown in Figure 4.3, consists of a complex white noise source, a delay block, and two complex summers. The delay block is used to introduce a delay to the signal to allow for synchronization with the despreader in the receiver. The delayed signal is then added with the complex white noise and any interference sources which are present. The main parameter for this block is the noise variance. This is used to control the noise power introduced to the system. The relationship between the noise PSD and the noise variance is

$$N_o = \frac{\sigma^2}{f_s} \tag{4.6}$$

where N_o is the noise PSD, σ^2 is the noise variance, and f_s is the sampling frequency. The second parameter, the code delay, is used to delay the signal by the specified number of samples.
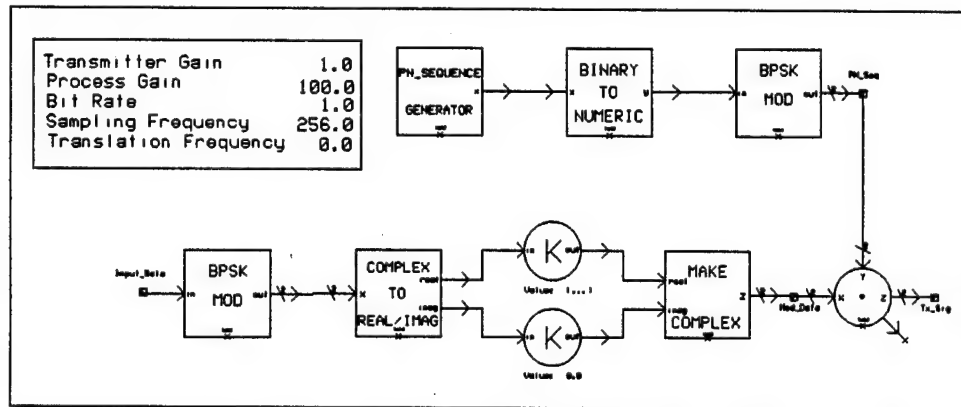
Figure 4.2   BPSK Direct Sequence Transmitter

The output of the channel is then used as the input to the DS-BPSK receiver shown in Figure 4.4. In addition, the receiver requires the PN sequence and the unspread modulated data as input. The PN sequence is used by the DS despreader shown in Figure 4.5. This eliminates the need for code synchronization and simplifies the despreading process. The despreader simply delays the PN sequence by the same delay as was present in the channel and multiplies it with the received data signal. The despread data is then passed onto a PSK matched filter demodulator. The output of the demodulator is then passed on to the PSK error counter. In addition, the original unspread modulated data, delayed

4-9
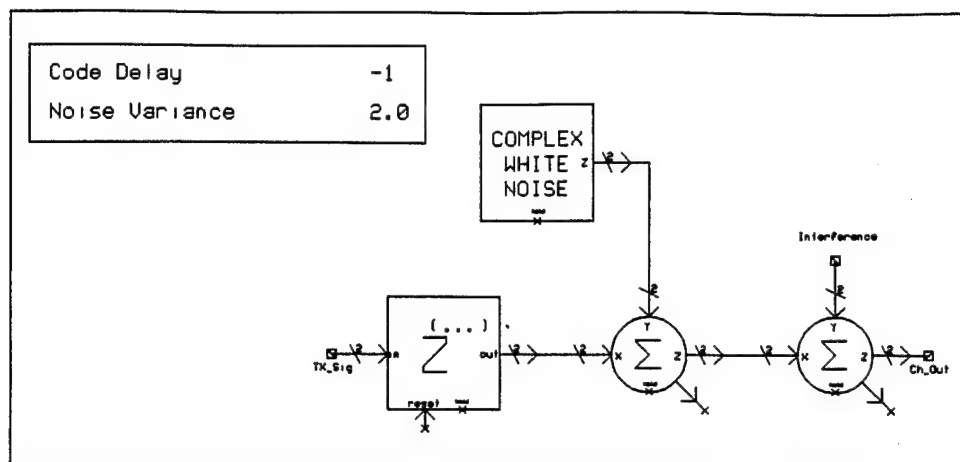
Figure 4.3   AWGN Channel Model

by the same amount as the channel delay, is also passed into the error counter. The error counter then compares the two data signals, computes the bit error rate, and writes it to a file. This allows bit error rates to be computed via the Monte Carlo or "Brute-Force" Method.
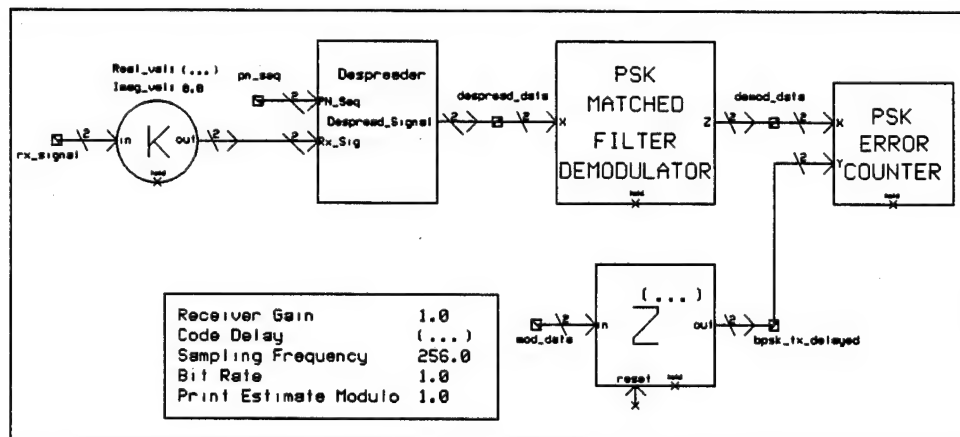
Figure 4.4   BPSK Direct Sequence Receiver

Due to the large number of simulations needed during this research, the Monte Carlo method was impractical, and the SPW Semi-Analytic Error Estimator Macro was used. This is a built in macro which estimates the bit error rate, over a given E_b/N_o range, by gradually incrementing the noise entering the system. For each noise increment, it recalculates the bit error rate, and at the end of the simulation generates a curve and data file. To use this macro, the noise variance of the channel was set

```
┌──────────────────────────────────────────────────────────────┐
│                                                                │
│                    ┌─────────────────────┐                     │
│                    │ Code Delay      0   │                     │
│                    └─────────────────────┘                     │
│                                                                │
│              ┌──────────┐           ┌──────────┐               │
│   PN_Seq     │ COMPLEX  │           │ ( . . . )│               │
│   ▣─\²─→  x  │          │ z ─\²─→ \²─→ in    out─\²─→          │
│              │          │           │    Z     │               │
│              │  CONJ    │           │          │               │
│              └────┬─────┘           │ reset  hold│              │
│                  hold               └──┬──────┬──┘              │
│                   x                    ▲     x                  │
│                                        x          ↓\²           │
│                                                  ╱─╲            │
│                                          Y──→   ╱ Y ╲           │
│                   ▣─\²─→  x  o  z ─\²─→ ▣      ╱  o  ╲          │
│                   Rx_Sig              │       ╲     ╱           │
│                                       hold     ╲   ╱            │
│                                        x    Despread_Signal     │
│                                                   x             │
│                                                                │
└──────────────────────────────────────────────────────────────┘
```

<div align="center">Figure 4.5   Direct Sequence Despreader</div>

to zero. Then, the output of the modulator and the despreader were imported to the Signal Calculator. The macro was then started with the modulated signal being used as the reference and the despreader output being used as the distorted signal. The bit error rate curve obtained for this system, with no interference, is shown in Figure 4.6. Also on thi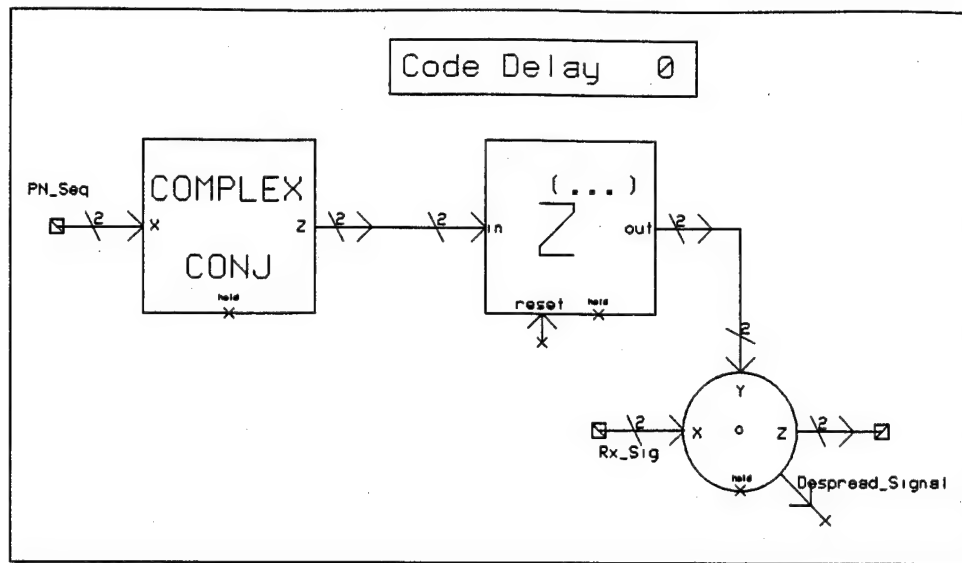s curve is the ideal bit error rate curve for a BPSK system. The proximity of our simulated results to the ideal results validates our DS-BPSK system.

4.6.2 **Jammer Model.** The interference source used for this research is shown in Figure 4.7. This source allowed for up to four jammer signals to be present at one time. In addition, it is capable of producing both continuous wave and pulsed jammers. The frequency, amplitude, duty cycle, and pulse repetition frequency (PRF) of each individual source can be controlled independently. Each jammer consists of a complex tone which is multiplied component wise by square waves. The square waves allow for the variation of the duty cycle and the PRF. It should be noted that the PRF values used in this research are scaled by the sampling frequency. This was necessary to facilitate the use of the lowpass simulations. The ratio of PRF/f_s must be used to relate these PRFs to the PRFs of real-world systems
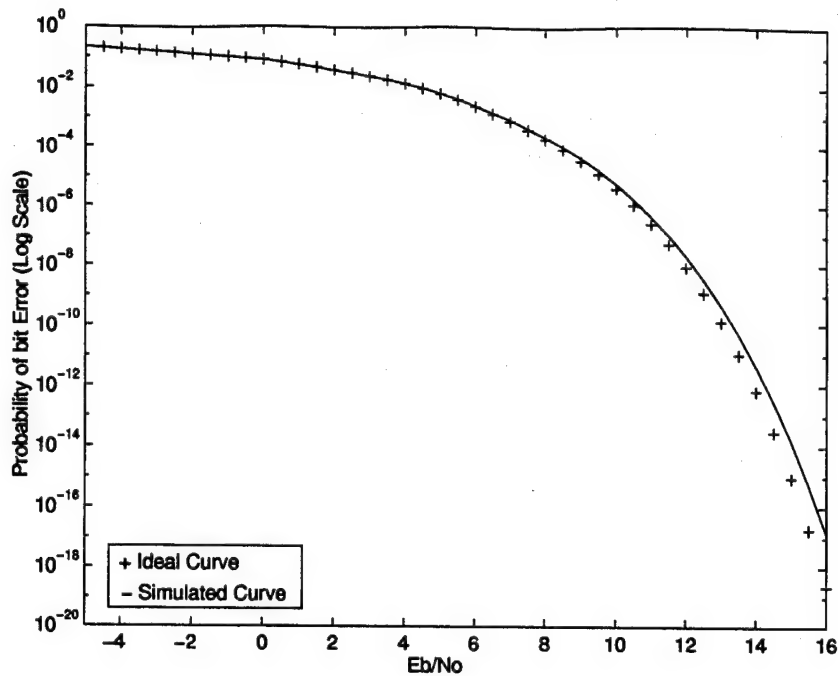
Figure 4.6   Simulated and Ideal BER Curve for BPSK System (AWGN w/ no Jammers)

operating at higher frequencies. Examples of the spectra of jammer waveforms which can be produced are shown in Figure 4.8.

4.6.3 **Wideband Radiometer.**   The wideband radiometer used in this research is shown in Figure 4.9. This interceptor operates on the principles discussed in Section 3.3.1 and simply estimates the energy content of a signal. This estimate is then compared to a threshold, and a decision is made accordingly. To estimate the energy, the block integrates the magnitude squared of the input signal. The output of the integrator is then scaled by $2/N_o$ and put into a sample and hold circuit. The sample and hold maintains the peak amplitude of the integration period while the threshold crossing counter determines whether or not a signal is present. If a signal is present, a counter is incremented.

Histograms for the sample and hold operation, shown in Figure 4.10, illustrate the distribution characteristics for the radiometer test statistic. When only noise is present, the distribution is centered about $2TW$. When signal and noise are both present, the distribution takes on the non-centrality
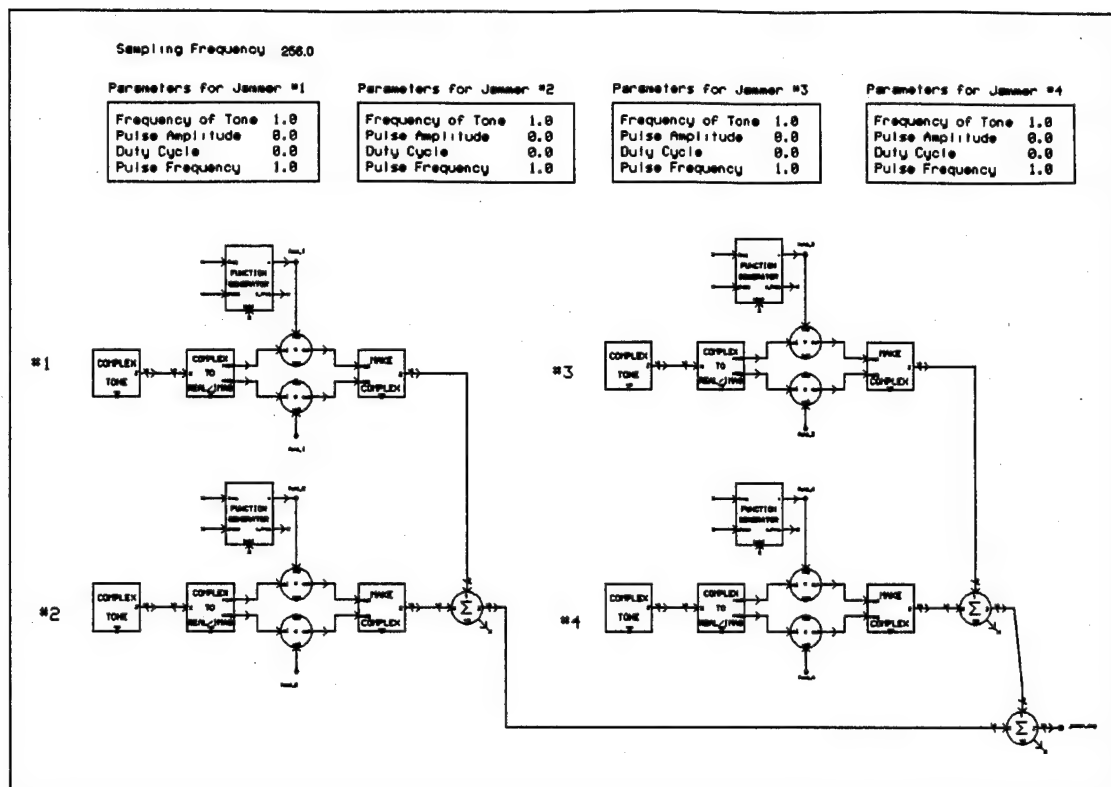
Figure 4.7   Jammer Model
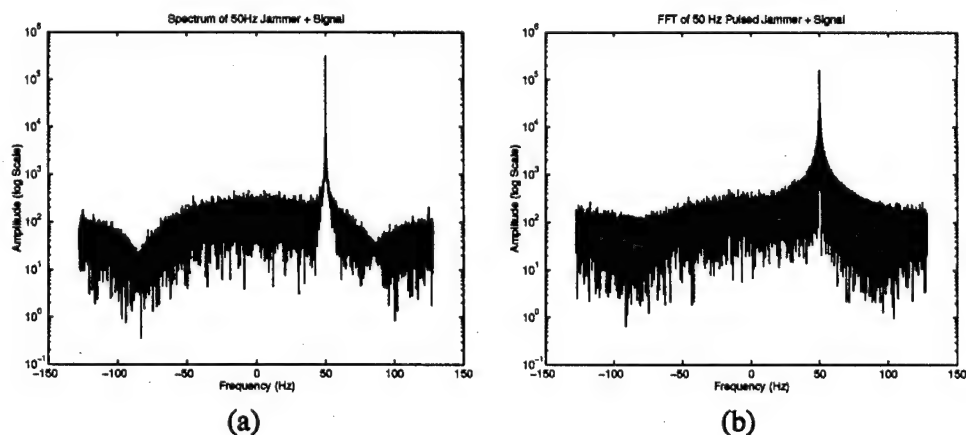

(a)

(b)

Figure 4.8   Spectra for DS-BPSK Signal with (a) a CW Jammer and (b) a Pulsed Jammer
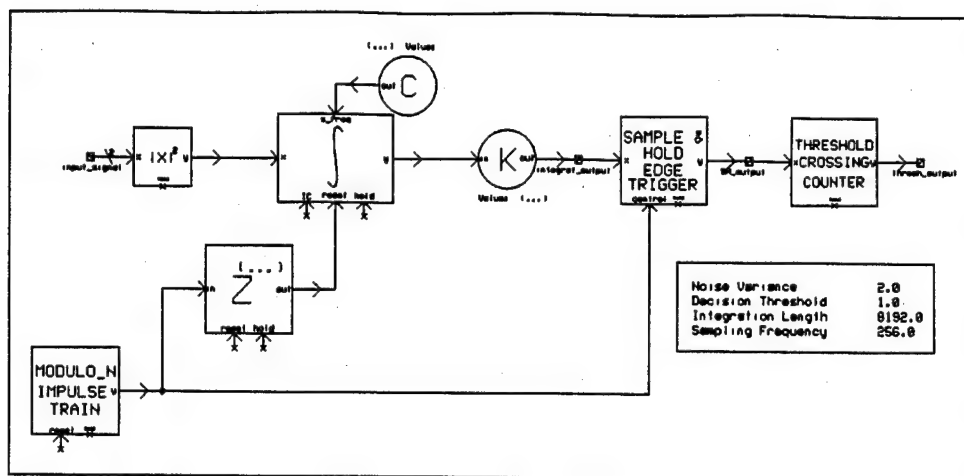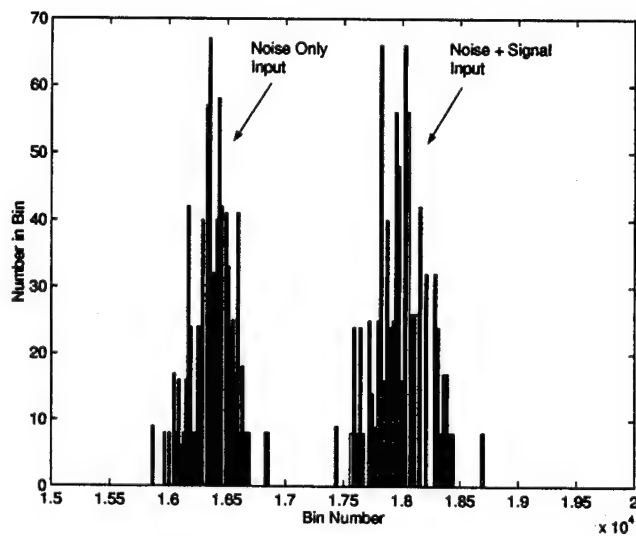
Figure 4.9   Wideband Radiometer

Figure 4.10   Histogram for the Radiometer
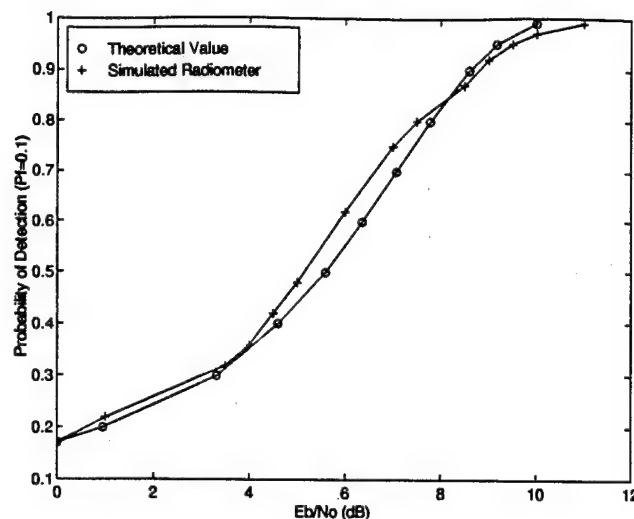
Figure 4.11   Theoretical and Simulated Radiometer ROCs

parameter of $2E_s/N_o$. In addition, Figure 4.11 shows the probability of detection as a function of the transmitted E_b/N_o for a $P_f = 0.1$. The values obtained through the SPW simulations are shown along with the values obtained from Equation 3.29. The small amount of error between the simulated and theoretical values helps to validate the operation of the radiometer model used in this research.

4.6.4 **Chip Rate Detectors.**   The two versions of chip rate detectors used in this research are shown in Figures 4.12 and 4.13. They operate on the principles discussed in Section 3.3.2 and estimate the energy present in the spectral spike produced by the delay and square operation. The chip rate detector in Figure 4.12 delays the received signal by one-half its chip rate and multiplies this by the non-delayed signal. This produces a spectral spike at the chip-rate which is isolated by a bandpass filter. The output of the filter is passed to a radiometer which estimates the energy present and decides whether or not a signal is present. The second version of the chip rate detector (MODAC), shown in Figure 4.13, operates under the same principle, but incorporates a noise floor reference. The noise reference loop operates under the assumption that the delay and multiply operation will not appreciably affect the interference sources (9). This results in the only difference between the noise reference and
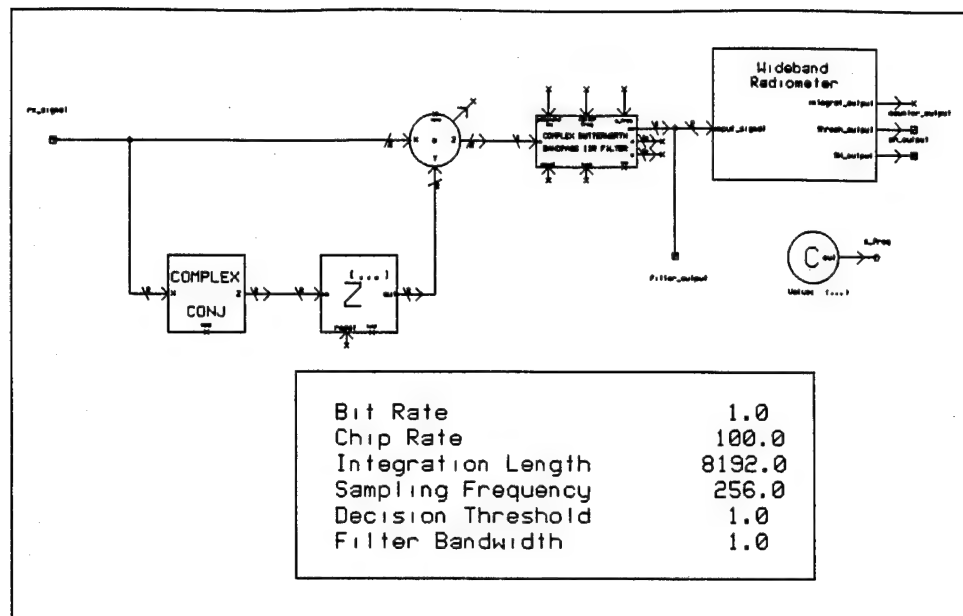
Figure 4.12   Chip Rate Detector
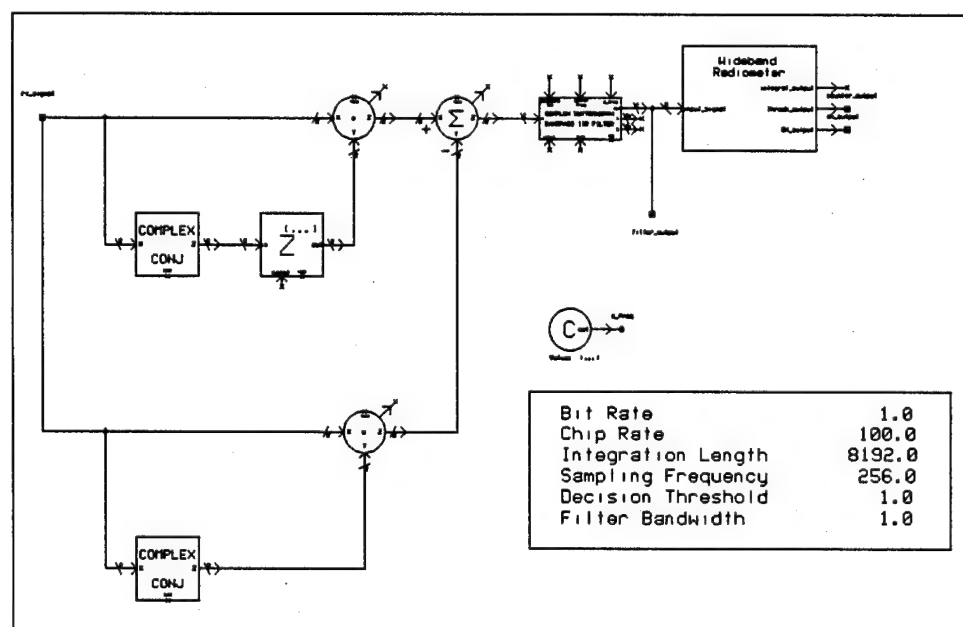
Figure 4.13   Chip Rate Detector with Noise Reference Loop (MODAC)

the signal reference being the spectral spike at the chip rate. By subtracting the two, the chip lines can be isolated and the radiometer can then be used to detect the presence of the signal.

The probability of detection versus the transmitted E_b/N_o for a $P_f = 0.1$ is shown in Figure 4.14. This figure shows the theoretical values obtained from Equation 3.37 as well as the simulated results. The simulated results for the chip-rate detector are very close to the theoretical values, and the simulated results for the MODAC are reasonably close. These curves help to validate both the chip-rate detector and the MODAC models used in this simulation. In addition, it illustrates the fact that in a no jammer situation, the MODACs performance is almost identical to that of the chip-rate detector.
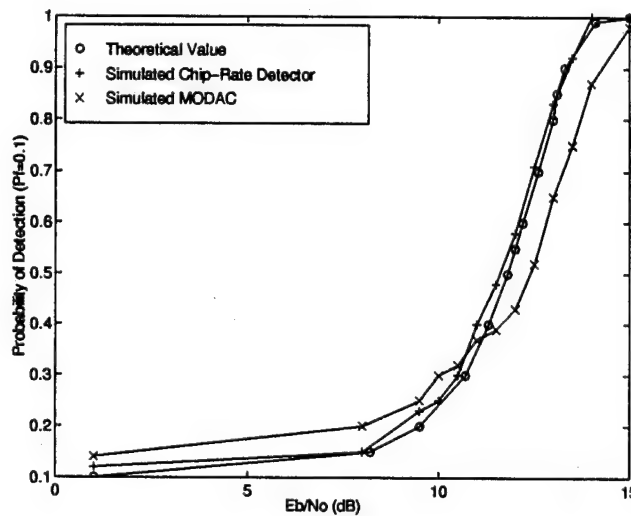
Figure 4.14   Theoretical and Simulated ROCs for the Chip-Rate Detector and the MODAC

4.6.5   **Digital Excision Filter.**   The digital excision filter, shown in Figure 4.15, is used to reduce the effects of the jammer upon the communication receiver and the interceptors. The digital excision filter (DEF) takes in a time signal which consists of noise, the spread data signal, and the jamming signal. The DEF is composed of three main sub-blocks, the data prep block, the excision filter, and the inverse data prep block. The first of these, the data prep block shown in Figure 4.16, decomposes the received signal into its real and imaginary components. The real and imaginary signals

4-17

are then made into vectors which were passed onto the FFT block. This block windows the data vector
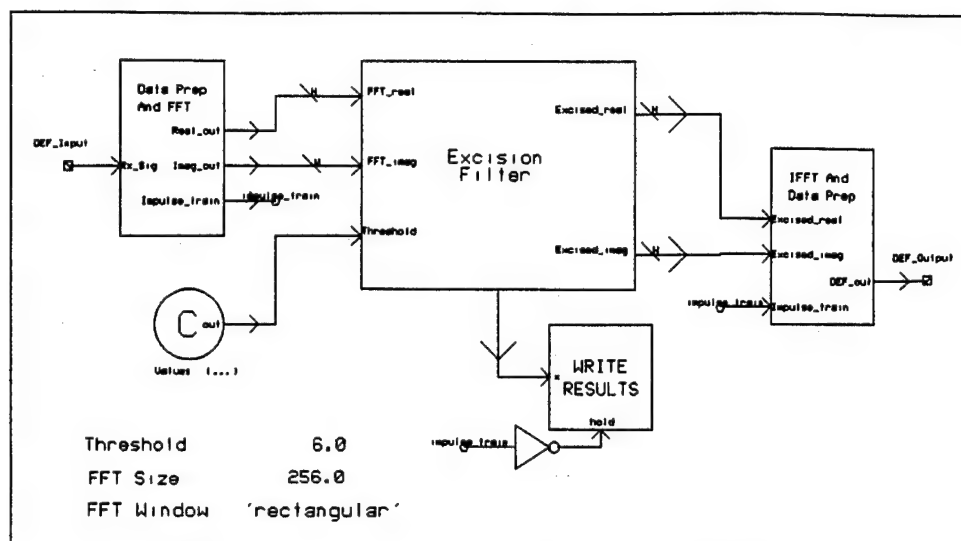
Figure 4.15   Digital Excision Filter

and performs an FFT according to

$$X(k) = \frac{1}{N} \sum_{n=0}^{N-1} x(n)e^{\left(\frac{-2\pi jkn}{N}\right)}$$

(4.7)

where $X(k)$ is the FFT of $x(n)$ and N is the length of the vector. The output of the data prep block is then passed to the excisor. This block is a custom-coded block (7) consisting of the block code in Appendix B. It computes the average signal level to which it adds a threshold value. It then removes any portions of the FFT which exceed this level. The threshold value used for all simulations was 6dB. This value was obtained from recommendations made in (4). The output of the excisor then enters the inverse data prep block. This block, shown in Figure 4.17, performs an inverse FFT (IFFT) according to

$$x(n) = \sum_{k=0}^{N-1} X(k)e^{\left(\frac{2\pi jkn}{N}\right)}$$

(4.8)

4-18
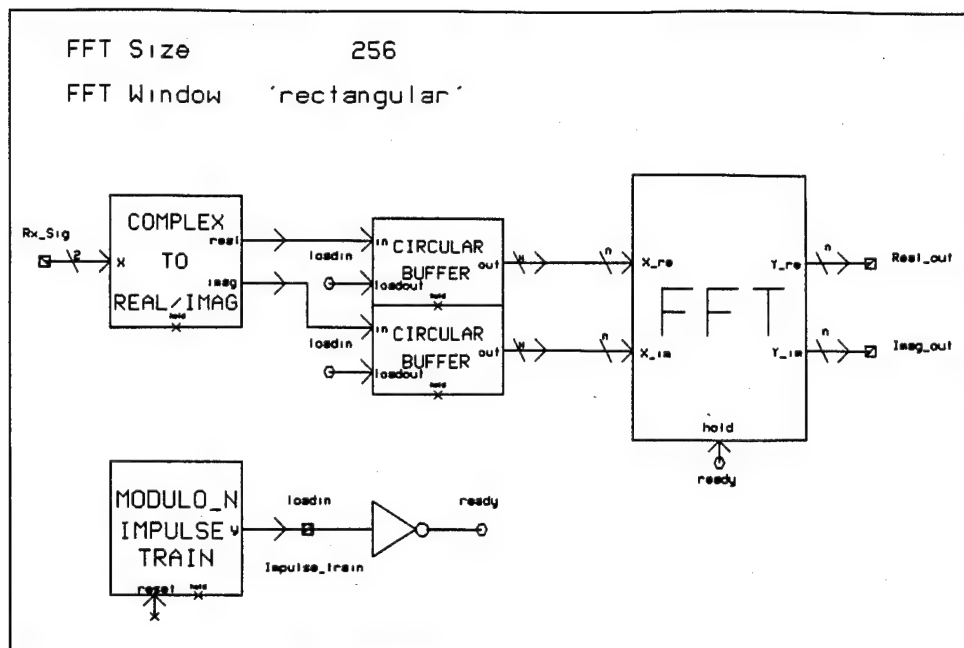
Figure 4.16   DEF Data Vector Preparation System

where $x(n)$ is the IFFT of $X(k)$ and N is the length of the vector. The vector output of the IFFT is then converted back to serial data. The real and imaginary serial signals are then converted back to a complex signal. This complex data is then passed on to the remainder of the system. Figure 4.18 illustrates the operation of the DEF. The output of the channel is the sum of the spread signal, noise, and a jammer signal. After passing through the DEF, the jammer tone has been excised while the remainder of the spectrum is unchanged.
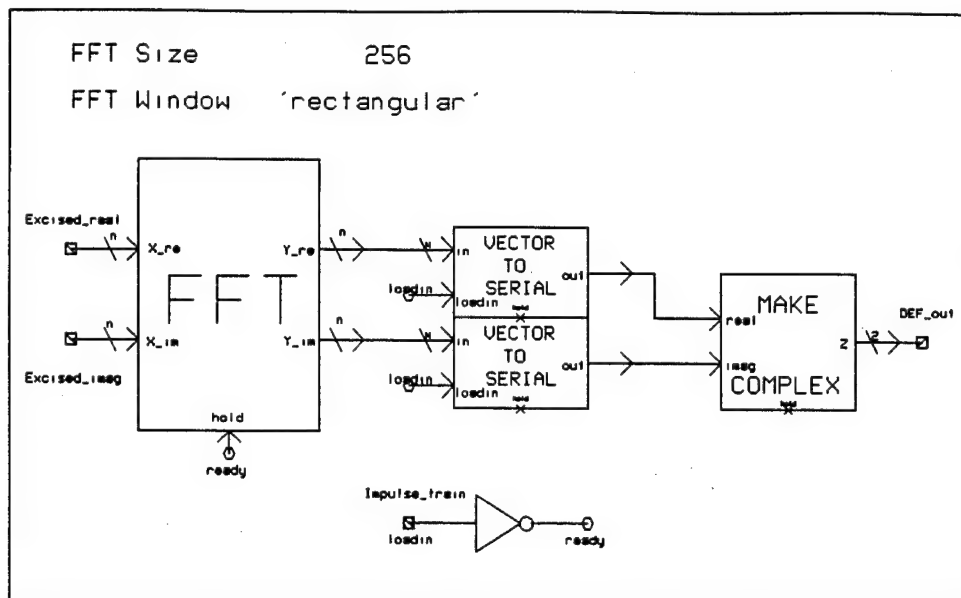
Figure 4.17   DEF Serial Data Preparation System
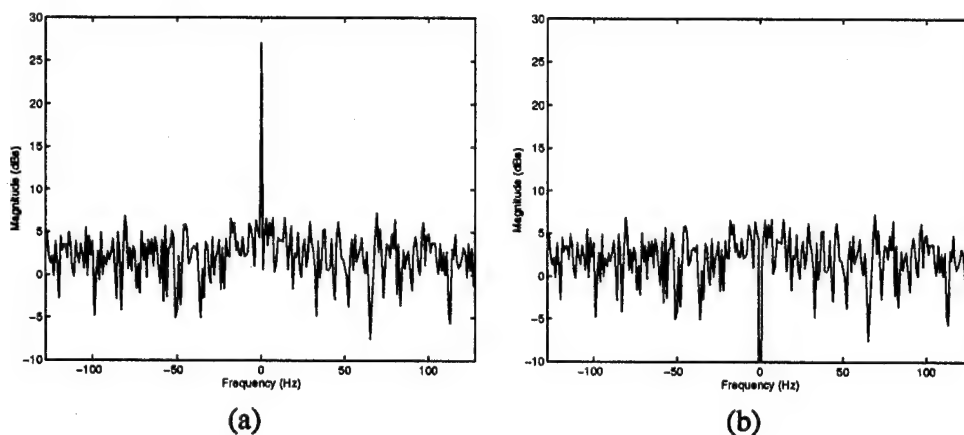
Figure 4.18   Spectra for (a) Output of Channel and (b) Output of DEF

V. Simulation Results and Analysis

5.1 Introduction

This chapter presents the reuslts of this research. It discusses the effects of both the CW and pulsed jammers, as well as the effects of the variation of the jammer paramters. Finally, it discusses the effects of the jammer paramters upon Q_{COMP}.

5.2 Simulation Parameters

In order to evaluate the performance of the DEF, simulations were conducted to test the system, both with and without the DEF, in the presence of single and multiple continuous wave and pulsed jammers. For the continuous wave jammers, shown in Table 5.1, all jammers had an amplitude of 31.62 with a 100% duty cycle. This gave us 1000W jammers which resulted in a 27dB jammer power to noise PSD ratio (J/N_o). The 1000W jammers were chosen because they greatly exceeded the jammer levels which could be handled by the SS capabilities of the system. For the pulsed jammers, shown in Table 5.2, all jammers had a pulse amplitude of 44.71, a duty cycle of 50%, and a pulse repetition frequency (PRF) of 0.0015. This gave the jammers an average power of 1000W and resulted in the same J/N_o. In addition to the above scenarios, the effects of the various jammer parameters were also simulated. These parameters were the frequency offset from the carrier, pulse repetition frequency, and duty cycle. By varying the jammer frequency, we were able to observe the effects of removing various portions of the spectrum up to the first null of the spread spectrum signal. The other two parameters allowed us to widen the bandwidth of the jammer and observe the effects of removing larger portions of the signal's spectrum.

The parameters which were required during the following simulations, as well as the values they were assigned, are listed below

- Sampling Frequency = 256Hz
- Code Delay = −255 with DEF, −1 without DEF

SCENARIO	NUMBER OF JAMMERS	PARAMETERS
1	1	Freq Offset (Hz): 0 Total Jammer Power: 1kW
2	1	Freq Offset (Hz): 50 Jammer Power: 1kW
3	2	Freq Offset (Hz): 0, 50 Jammer Power: 2kW
4	2	Freq Offset (Hz): 30, 70 Jammer Power: 2kW
5	3	Freq Offset (Hz): 0, 30, 70 Jammer Power: 3kW
6	3	Freq Offset (Hz): 30, 50, 70 Jammer Power: 3kW

Table 5.1   Continuous Wave Jammer Scenarios

SCENARIO	NUMBER OF JAMMERS	PARAMETERS
1	1	Freq Offset (Hz): 0 Total Jammer Power: 1kW
2	1	Freq Offset (Hz): 50 Jammer Power: 1kW
3	2	Freq Offset (Hz): 0, 50 Jammer Power: 2kW
4	2	Freq Offset (Hz): 30, 70 Jammer Power: 2kW
5	3	Freq Offset (Hz): 0, 30, 70 Jammer Power: 3kW
6	3	Freq Offset (Hz): 30, 50, 70 Jammer Power: 3kW

Table 5.2   Pulsed Wave Jammer Scenarios (PRF=.0015 and Duty Cycle=50%)

- Bit Rate = 1Hz

- Processing Gain = 100Hz

- Transmitter Gain = variable depending on desired E_b/N_o

- Noise Variance = 2.0

- Jammer Pulse Frequency = variable

- Jammer Frequency = variable

- Integration Length = 8192 samples (32 bit collect time)

- FFT Size = 256

- FFT Window = Rectangular

5.3   Effects of Jammer Parameter Variations

As previously stated, it was desired to observe the performance of the communication system as a function of various jammer parameters. These parameters were the offset from the center frequency, the pulse repetition frequency, and the pulse duty cycle. These results are shown in Figure 5.1 for an E_b/N_o of 9.5dB. The first parameter variation, the jammer frequency offset, was performed with a 1000W continuous wave jammer. For the PRF variation, the jammer was a pulsed tone jammer at 0Hz (0Hz was the carrier due to the Lowpass Simulation). It had a 50% duty cycle, and the amplitude of the tone was adjusted to maintain an average power of 1000W. The duty cycle variation was also performed with a pulsed tone jammer located at 0Hz, with a constant PRF of 0.01 and an average power of 1000W. The first thing to be observed in these results helps to demonstrate the consistency of the BER simulations using the semi-analytic error estimator. For the CW jammer at 0Hz, the BER was 7.328×10^{-5}. This is identical to the value obtained for the BER for the 100% duty cycle pulsed jammer simulation. In addition, for the pulsed jammer with a PRF of .0005, which approximates a CW jammer, the BER was 7.326×10^{-5}. Finally, for the pulsed jammer with a PRF of 0.01, the BER value was 2.021×10^{-3}. This is consistent with the value, obtained from the duty cycle variation simulation, for a duty cycle of 50%. These values help to validate the use of the semi-analytic error estimator.

(a)

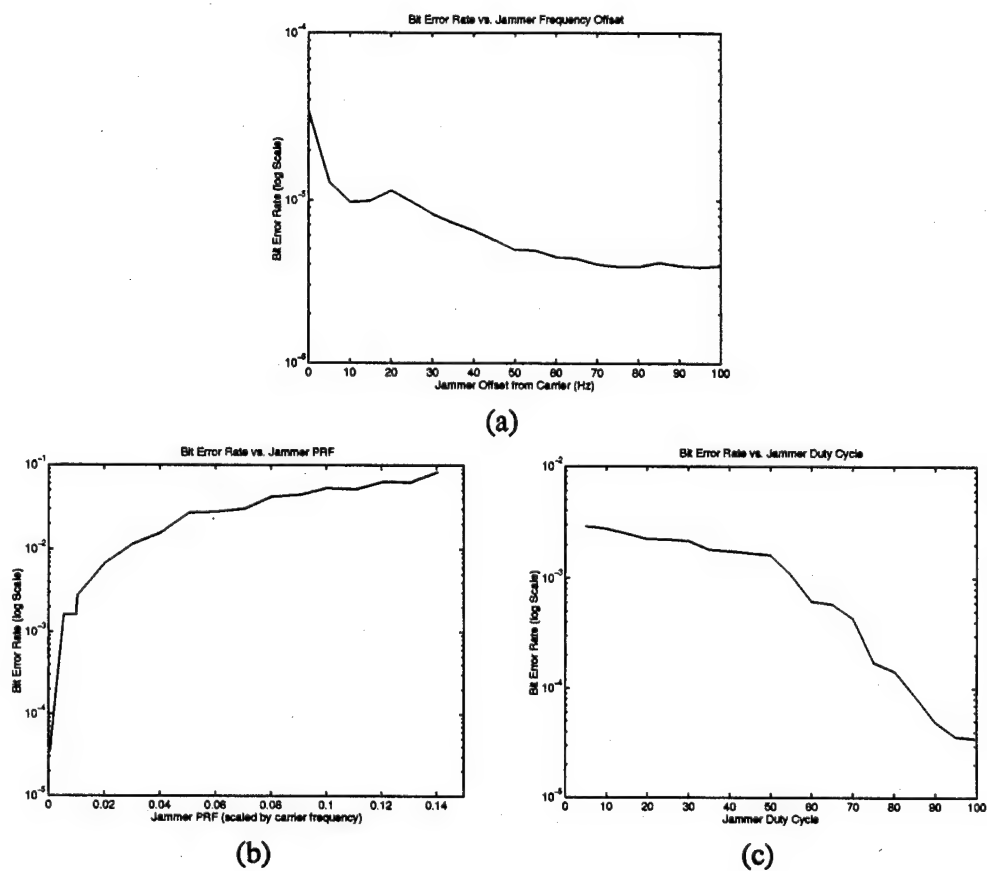(b)   (c)

Figure 5.1   Effects of Jammer Parameters for (a) Jammer Offset, (b) Jammer PRF, and (c) Jammer
             Duty Cycle

The plots themselves are consistent with the results that were intuitively expected. For the jammer offset, the BER decreased as the jammer offset was increased. After reaching 50Hz offset, the remaining BER values were reasonably close to the ideal BER values. As expected, there was a sharp decrease immediately after the first few increments from 0Hz. This decrease is due to the removed portion of the signal spectrum moving away from the peak of the signal spectrum. If the peak of the main lobe of the data signal is removed, more information is removed than if areas around the nulls of the spectrum are removed.

The PRF results are also consistent with the expected results. As the PRF increased, the width of the jammer pulse was increased, and the DEF must remove a larger portion of the signal spectrum. This resulted in a sharp increase in BER. After the PRF reached a value of 0.0405, the BER for all E_b/N_o values had decreased to a value on the order of 10^{-2}. For PRFs below 0.0014, the DEF performance was satisfactory, and for PRFs below 0.0013, the results were consistent with those obtained for the CW jammers. For the duty cycle variation, the BER was decreased as the duty cycle increased. This corresponds to the expected results. As the jammer pulse width decreases, its spectrum widens and its effect upon the BER are increased.

5.4 Effects of Continuous Wave Jammers

The results of the CW jamming scenarios are shown in Figures 5.2 through 5.7. The BER curves are consistent with the expected results and concur with the results obtained from the jammer offset simulation in the previous section. In all scenarios, the DEF performed very well and excised almost 100% of the jammer tone. The greatest increases in BER occurred whenever a jammer was located at 0Hz. This forced the DEF to remove the center of the data spectrum. When the data signal was despread, this resulted in removal of a large portion of the data signal's main lobe. As the jammers were moved to frequencies away from 0Hz, the removed portion of the spectrum corresponded to portions further away from the peak of the de-spread data's main lobe. This produced a decrease in

the overall effects of the jammer and allowed results to approach ideal values. As additional jammers were introduced, once again larger portions of the spectrum were removed. As expected, this produced an increased BER.

For the CW scenarios, the DEF allowed all interceptors to operate effectively. The radiometer showed the best performance and showed no degradation between single and multiple jammers. The chip-rate detector and MODAC showed a slight decrease in performance for multiple jammers. This is most likely due to the presence of the small portions of un-removed jammer signals reducing the detectability of the spectral line produced through the delay and multiply process. The spectral line produced by both of these interceptors will contain a relatively constant amount of energy. The un-removed jammer signals will introduce additional energy that will reduce the relative difference between the reference threshold and the energy contained in the spike. In Figures 5.2 through 5.7, the Interceptor ROCs are shown for a transmitted E_b/N_o of 17dB.

Figure 5.2 Results of CW Jammer Scenario 1: (a) System BER (b) Radiometer ROC (c) Chip Detector ROC (d) MODAC ROC

(a)

(b)

(c)

(d)

Figure 5.3   Results of CW Jammer Scenario 2: (a) System BER (b) Radiometer ROC (c) Chip Detector ROC (d) MODAC ROC

(a)

(b)

(c)

(d)

Figure 5.4   Results of CW Jammer Scenario 3: (a) System BER (b) Radiometer ROC (c) Chip
Detector ROC (d) MODAC ROC

Figure 5.5 Results of CW Jammer Scenario 4: (a) System BER (b) Radiometer ROC (c) Chip Detector ROC (d) MODAC ROC

Figure 5.6 Results of CW Jammer Scenario 5: (a) System BER (b) Radiometer ROC (c) Chip Detector ROC (d) MODAC ROC
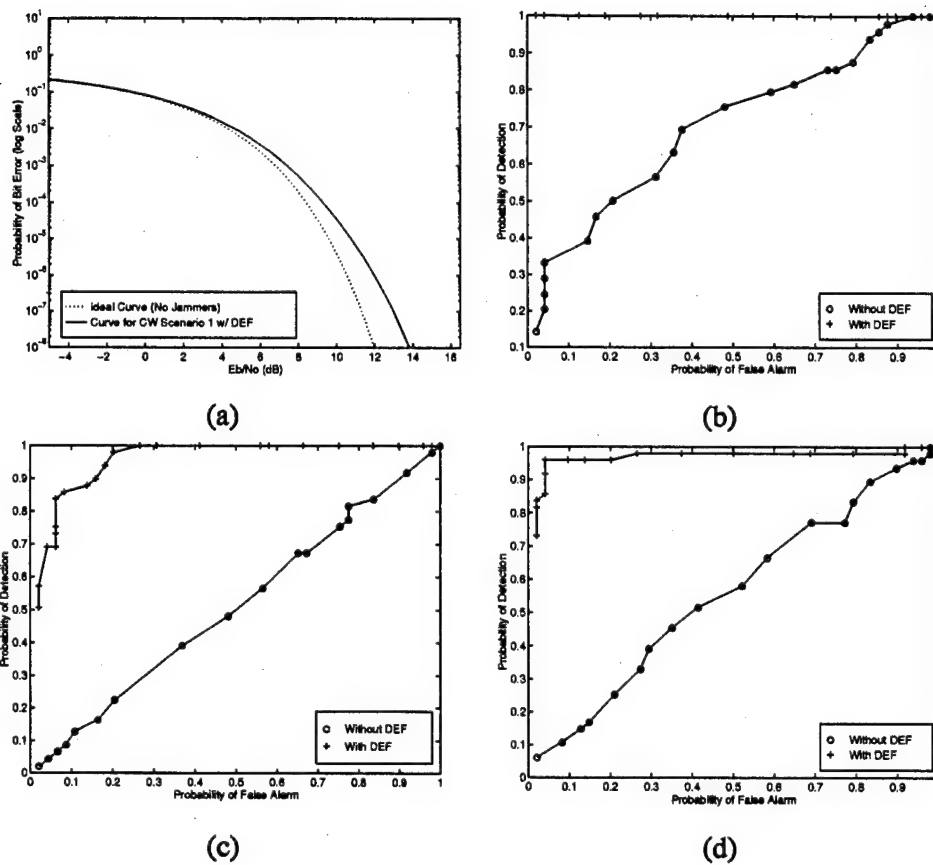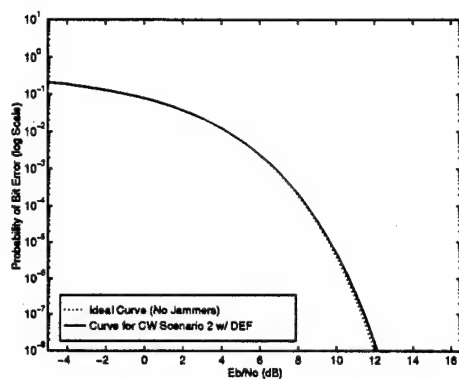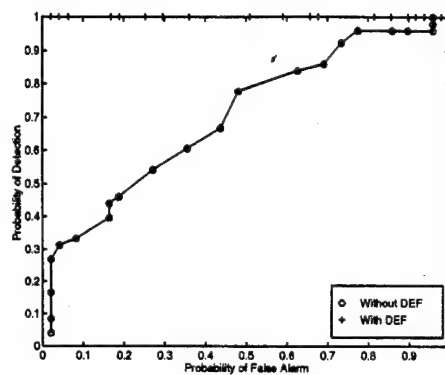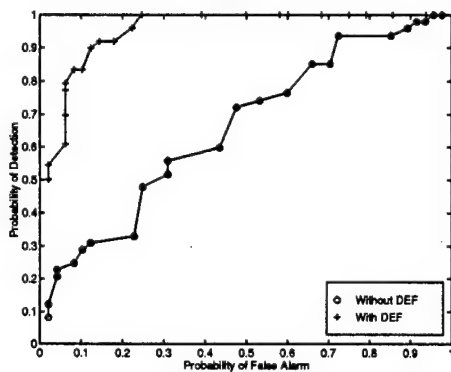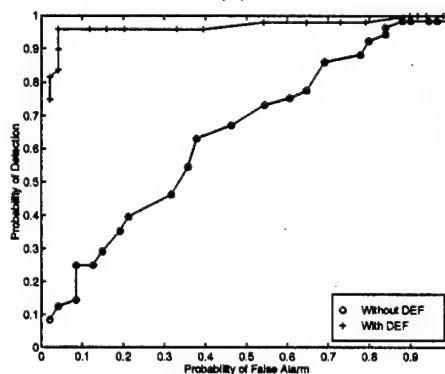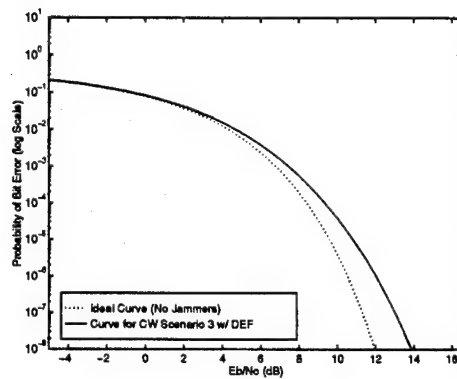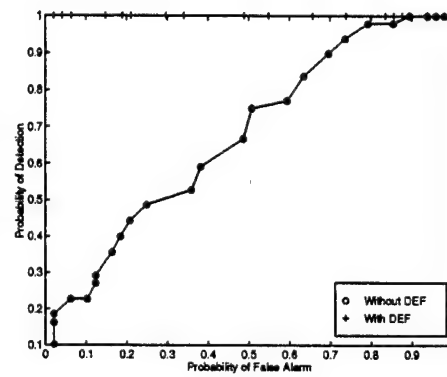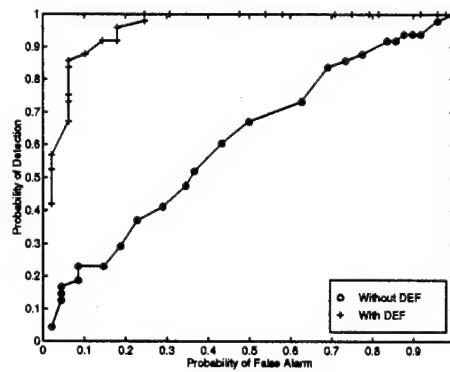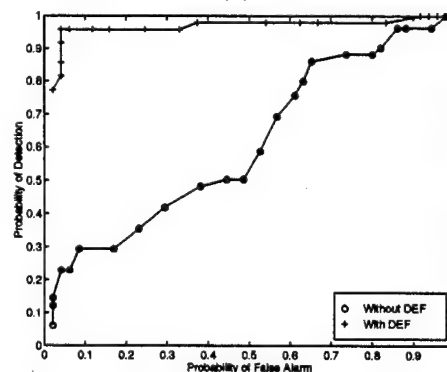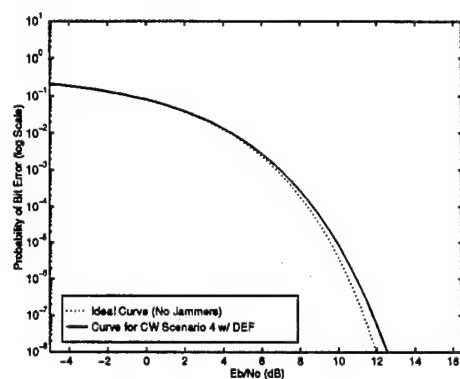
Figure 5.7   Results of CW Jammer Scenario 6: (a) System BER (b) Radiometer ROC (c) Chip Detector ROC (d) MODAC ROC

5.5 Effects of Pulsed Jammers

The results obtained for the pulsed jammer scenarios are shown in Figures 5.9 through 5.14. The curves obtained were inconsistent with the expected results. The BER curves remained fairly constant with little variation being introduced by the frequency location of the jammer. This was inconsistent with the results that were expected using the data obtained in Figure 5.1. It is suspected that even though the jammers in scenarios 2, 4, and 6 were located away from the center frequency, they still forced the DEF to remove a relatively wide portion of the data signal's spectrum. This portion is sufficient to markedly degrade the BER regardless of its location. Because of limitations introduced by the length of time required for simulations with high sampling frequencies, the simulation bandwidth used in this research was approximately 2.5 times the chip rate. This limited the frequencies at which jammers could be placed. Larger simulation bandwidths might show that if the pulsed jammers are placed at frequencies outside of the main lobe of the spread data, the results would begin to approach those that were expected. The ROC curves, obtained for the interceptors in the presence of the pulsed jammers, were also noticeably degraded. At first, the ROCs were plotted for a transmitted E_b/N_o of 17dB. This resulted in severely degraded ROC curves for all of the pulsed jammer scenarios, regardless of the jammer's frequency or the presence of the DEF. Upon inspection of the sample and hold data for the interceptors, shown in Figure 5.8 for the MODAC, the cause of the degradation was readily apparent. In part (a) of Figure 5.8, the sample and hold is shown when no filter is present. The actual jammer pulses are easily seen, as well as the large differences in the sample value that they produce. In part (b) of Figure 5.8, the large spikes that occur in the sample and hold value coincide with the jammer pulse transitions. These spikes are produced by the DEF during the filtering process. When the integration period contains one of these spikes, the corresponding sample and hold value is considerably larger than the surrounding values. In order to obtain acceptable detection rates, the received signal power must be large enough to raise the 'signal + noise' sample values above the spikes. In an attempt to reduce the effect of these spikes, a clipper block was added to the output of the DEF. This clipper block
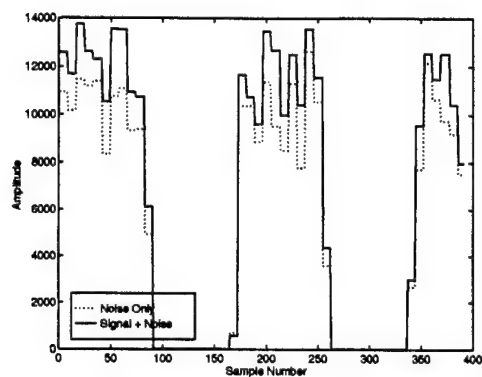
(a)
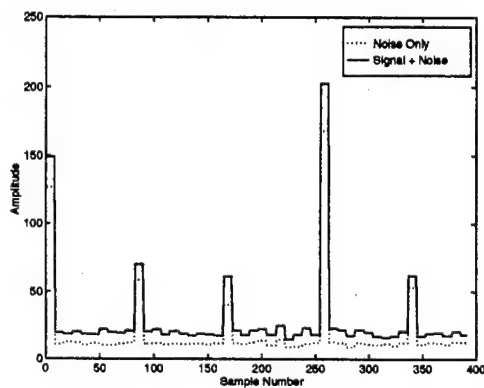
(b)
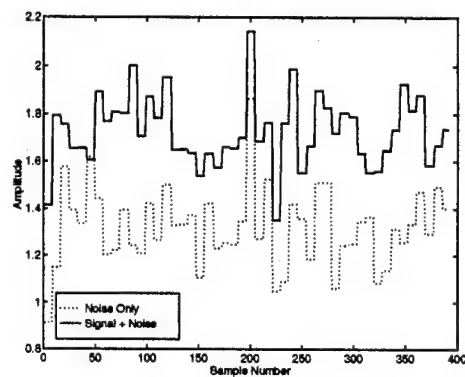
(c)

Figure 5.8   Example of Sample and Hold Data for Pulsed Jammer with (a) No Filter, (b) DEF, and (c) DEF and Clipping Circuit

limited the amplitude of the spikes and allowed the 'signal + noise' sample values to raise above the 'noise only' samples for smaller E_b/N_o values. Initial simulations were run with the clipper set to the maximum expected noise value. Additional research is still needed to determine whether lower values would further improve performance. This resulted in sample values, shown in part (c) of Figure 5.8, which were more uniform in level.

In Figures 5.9 through 5.14, the ROCs are shown for the interceptors with no filter, the original DEF, and the DEF with the clipping. The radiometer was able to perform fairly well with an E_b/N_o of 17dB; however, the chip rate detector and MODAC both required approximately 22dB to achieve acceptable performance. This difference in performance was due to the relative difference between the 'signal + noise' samples and the 'noise only' samples. The radiometer produced the greatest difference between these levels and was able to raise the 'signal + noise' samples to a value high enough to overcome the spikes with a lower received E_b/N_o. The chip rate detector produced the next largest difference in sample levels, with the MODAC producing the smallest difference. Because of these smaller differences, more E_b/N_o was required.

A very important observation to be made pertains to the shape of the ROCs when the DEF was used, and when the DEF plus clipper was used. While the DEF appears to be producing reasonably good curves for the radiometer, it should be noted that the ROC makes a sudden transition to the 0.90 and above P_d range. This transition occurs when there is enough E_b/N_o present to push the majority of the 'signal + noise' samples above the 'noise only' samples. However, to achieve these P_d values for small P_f (less than 0.1) large increases in E_b/N_o would be required to overcome the spikes present in the sample and hold values. The same observation should be made for the chip rate detector and MODAC. After making these observations, one should then note the shape of the ROC when the DEF plus clipper is used. These curves produce the gradual transition that is expected in a proper ROC curve. This allows the higher P_d values to be obtained, for the smaller P_f values, with smaller increases in E_b/N_o.
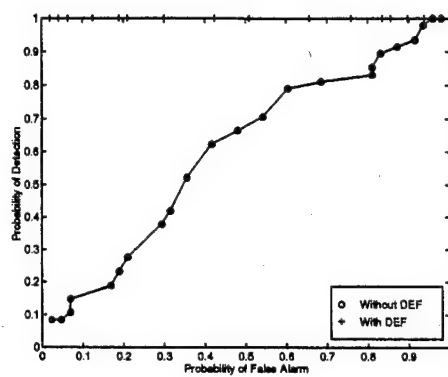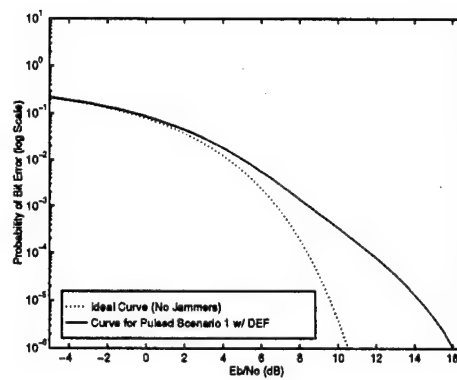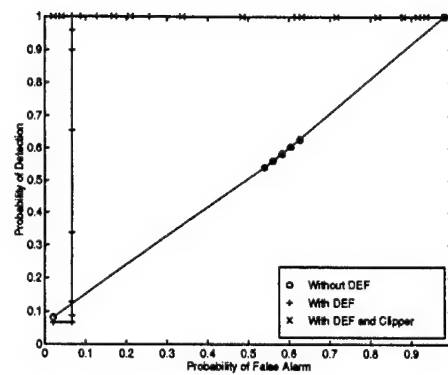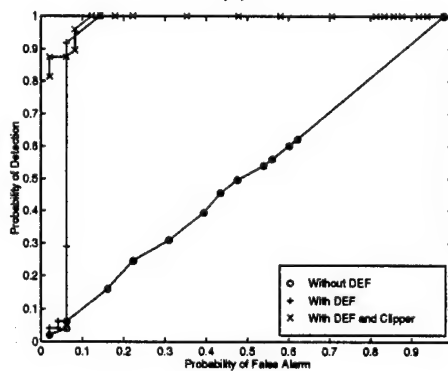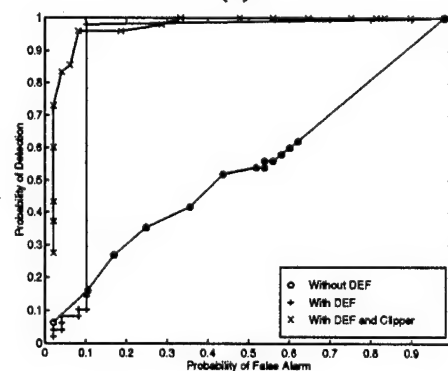
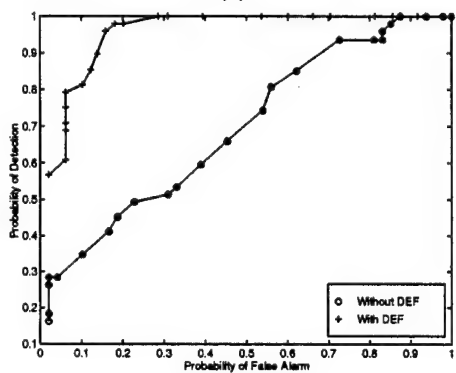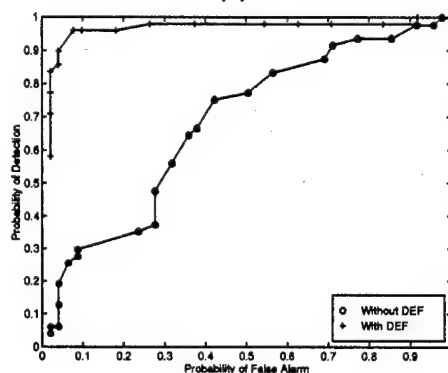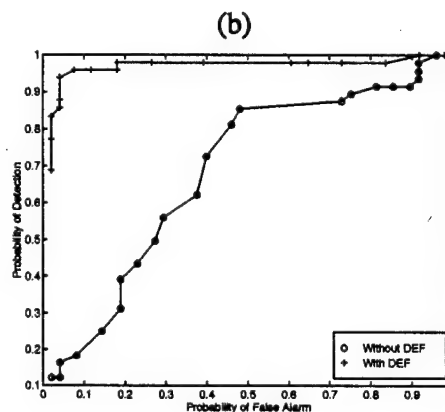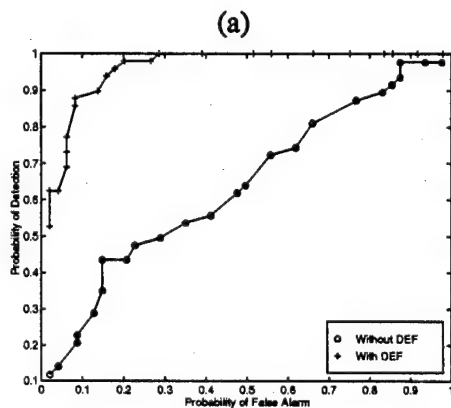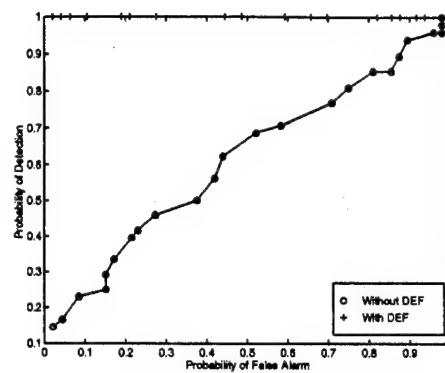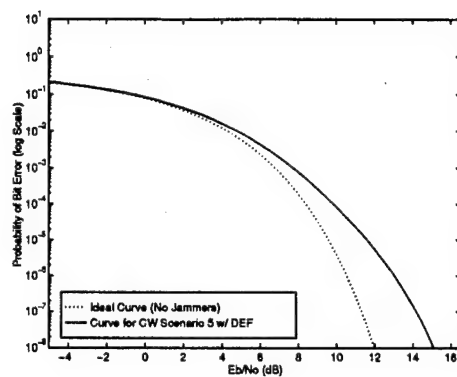Figure 5.9 Results of Pulsed Jammer Scenario 1: (a) System BER (b) Radiometer ROC (c) Chip Detector ROC (d) MODAC ROC
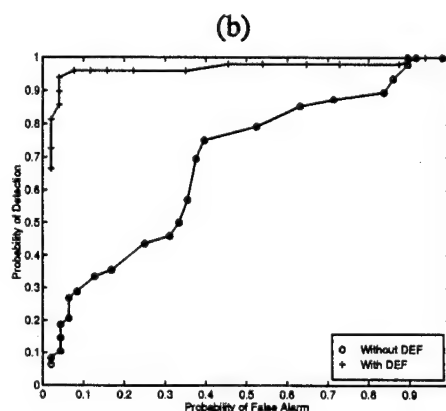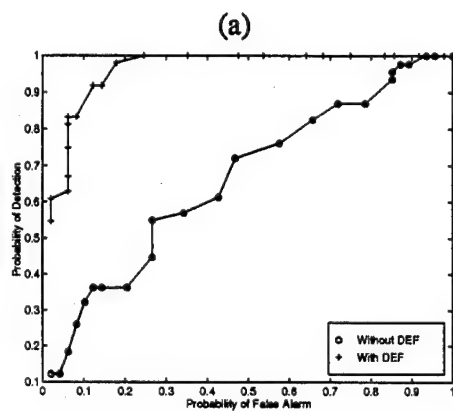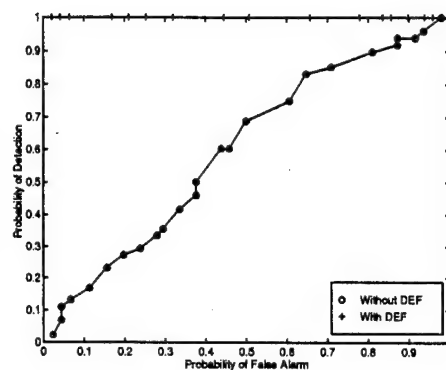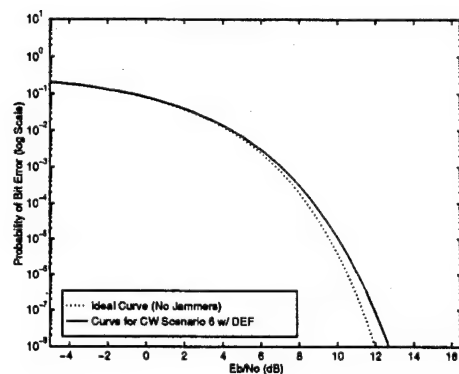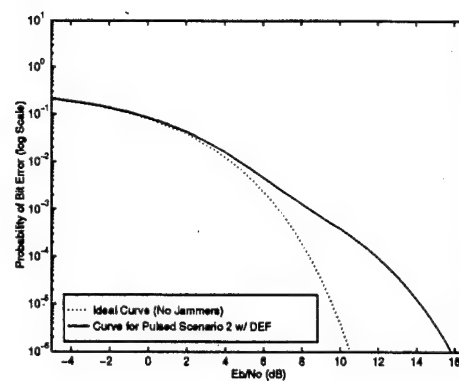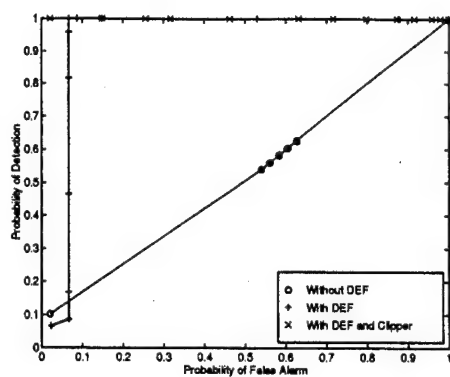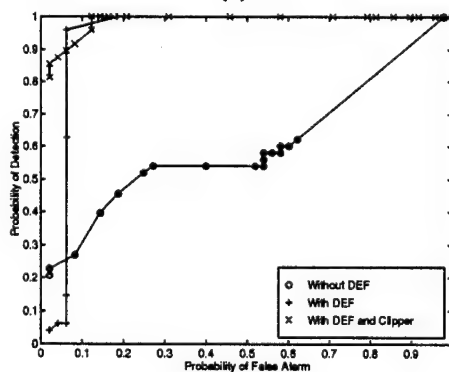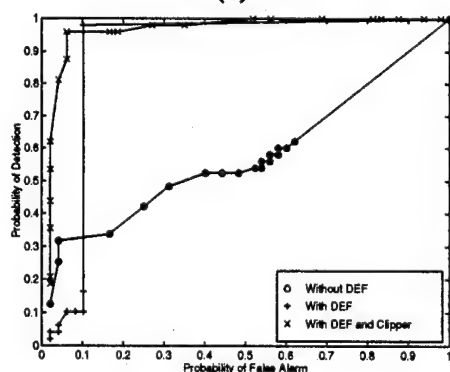
Figure 5.10 Results of Pulsed Jammer Scenario 2: (a) System BER (b) Radiometer ROC (c) Chip Detector ROC (d) MODAC ROC
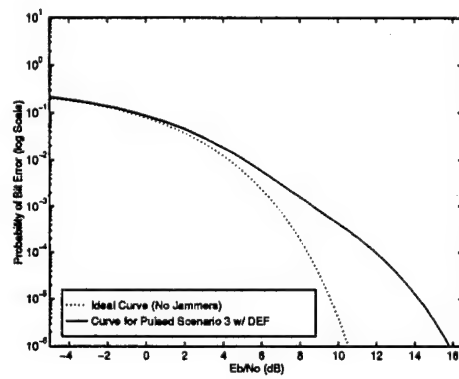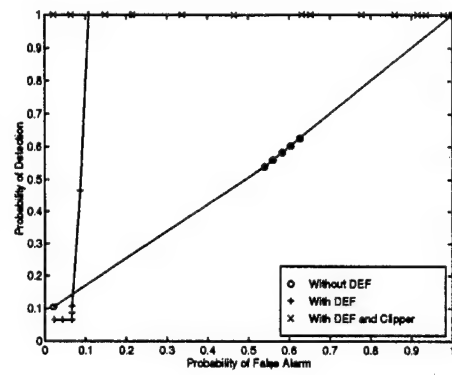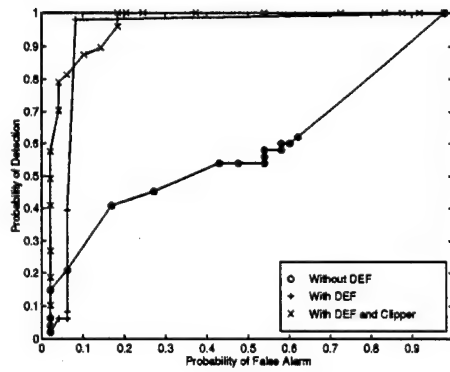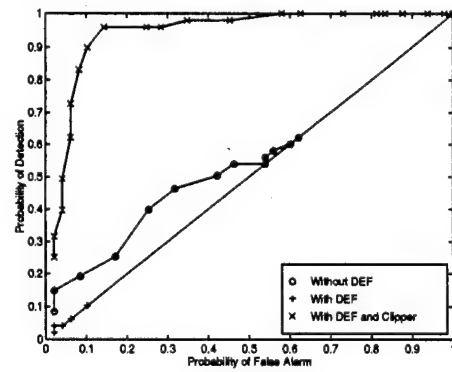
Figure 5.11   Results of Pulsed Jammer Scenario 3: (a) System BER (b) Radiometer ROC (c) Chip Detector ROC (d) MODAC ROC
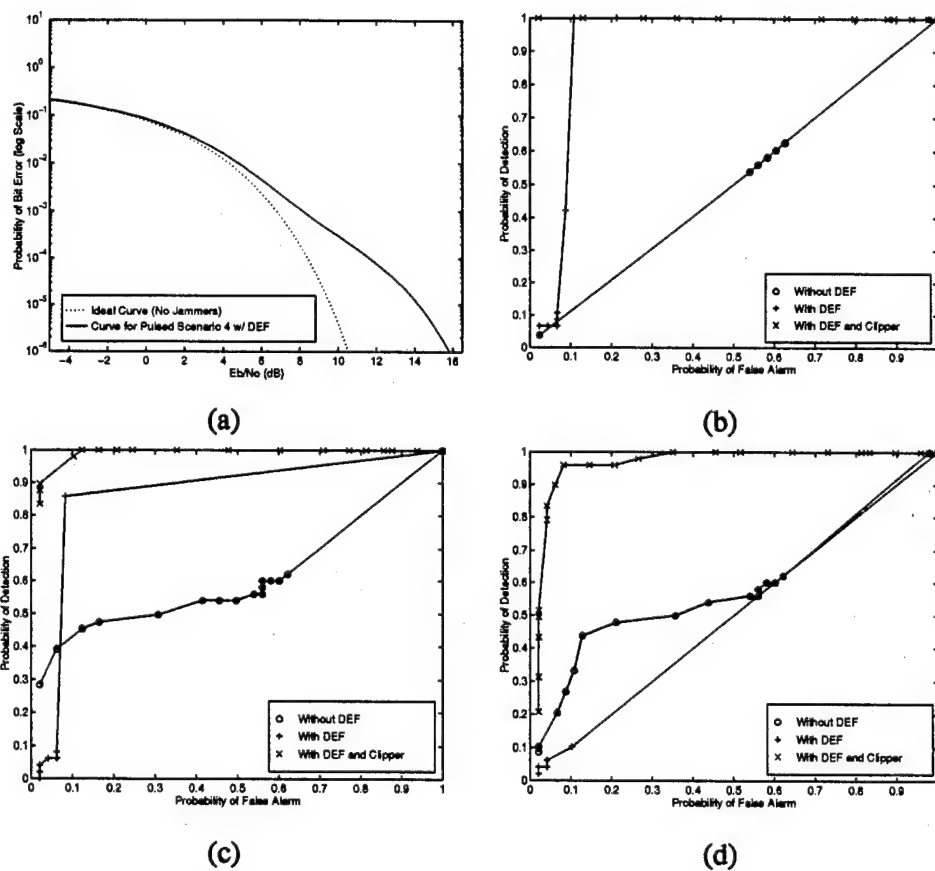
Figure 5.12 Results of Pulsed Jammer Scenario 4: (a) System BER (b) Radiometer ROC (c) Chip Detector ROC (d) MODAC ROC

(a)

(b)

(c)

(d)
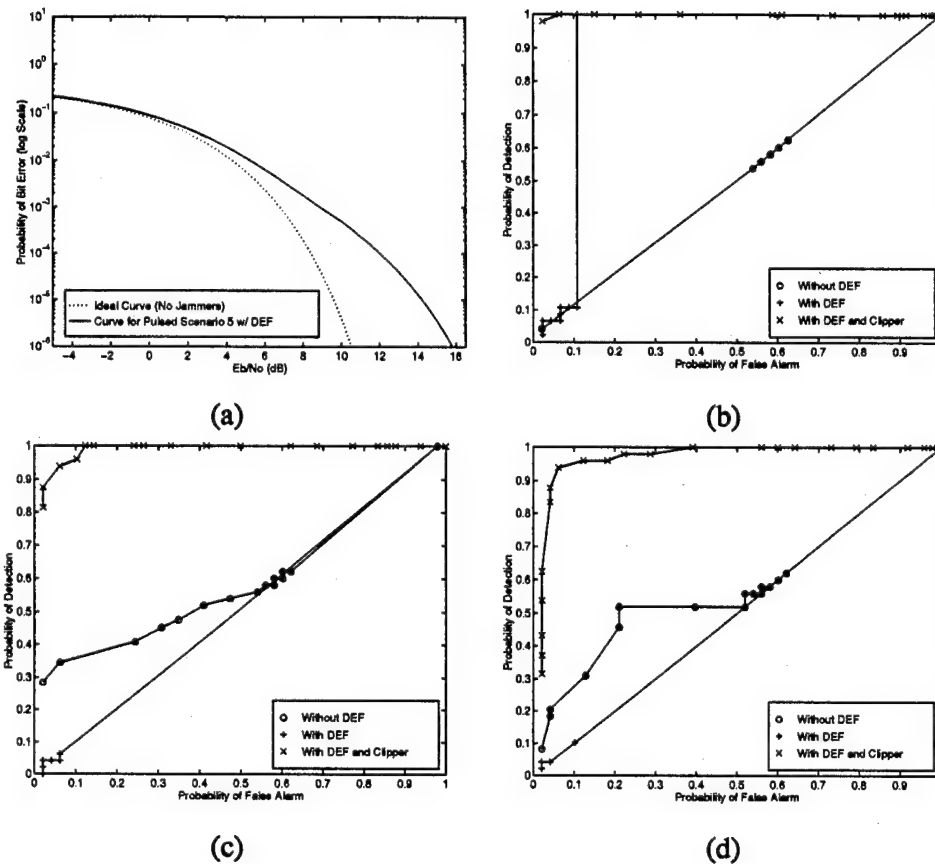
Figure 5.13   Results of Pulsed Jammer Scenario 5: (a) System BER (b) Radiometer ROC (c) Chip
Detector ROC (d) MODAC ROC
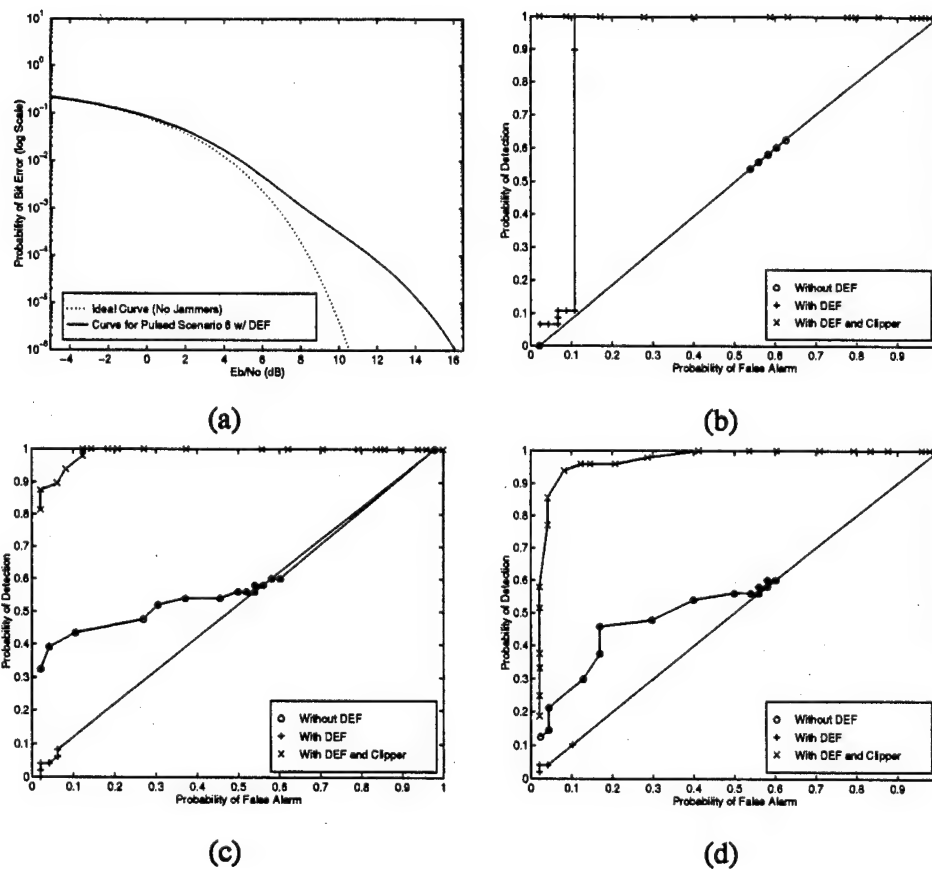
Figure 5.14   Results of Pulsed Jammer Scenario 6: (a) System BER (b) Radiometer ROC (c) Chip Detector ROC (d) MODAC ROC

5.6 Composite Quality Factor

As presented in Chapter III, the composite quality factor is a means of comparing the transmitted signal powers required by the communication receiver and the interceptor to maintain an acceptable performance level. This quality factor is significant because it deals only with the type of detection and modulation employed. It is independent of parameters such as the transmission channel, antenna gains, and integrates the interference suppression benefits of the DEF. Any factors which raise the signal power to noise PSD ratio (S/N_o) required by the intercept receiver will increase the composite quality factor. Conversely, any factors which increase the S/N_o required by the communication receiver will decrease the modulation quality factor.

The composite quality factor for this system was first obtained as a function of the jammer offset frequency. The resulting values, shown in Table 5.3, illustrate the behavior of the modulation quality factor as the jammer frequency is gradually moved away from the center frequency. These values were obtained for a P_d of 0.95, a P_f of 0.10, and a P_e of 1×10^{-5}. In addition, values are shown for each intercept receiver used. As expected, the values gradually increase as the jammer offset increases. This

Jammer Offset	Composite Quality Factor (dBs)		
	Chip-Rate Detector	MODAC	Radiometer
0Hz	7.69	8.19	1.69
20Hz	8.40	8.90	2.40
40Hz	8.65	9.15	2.65
60Hz	8.81	9.31	2.81
80Hz	8.87	9.37	2.87
100Hz	8.86	9.36	2.86

Table 5.3   Composite Quality Factor for Various Jammer Offset Values

is due to the S/N_o required for a given BER gradually decreasing as the jammer move away from the center frequency. This result is expected and follows the curve in part (a) of Figure 5.1. The S/N_o required by the interceptors is relatively constant and is not a function of the jammer offset frequency. This is because the DEF is able to effectively remove the CW jammer tone regardless of its frequency.

After the jammer has been removed, the interceptors are still able to detect the signal regardless of which portion of the spectrum was removed.

Next, the composite quality factor was investigated as a function of the jammer duty cycle and PRF. As these parameters of the pulsed jammer were varied, the effects they produced upon the S/N_o required by the interceptor were often quite large. This was due to the problem discussed in the previous section on the effects of the pulsed jammers. The values obtained are shown in Tables 5.4 and 5.5. Once again, these values were obtained for a P_d of 0.95, a P_f of 0.10, and a P_e of 1×10^{-5}. In both of these tables, the DEF and the DEF plus clipper were used on both the communication and intercept receiver. In the cases tested for the MODAC, the DEF plus clipper provided approximately 10dB of improvement over the DEF when the PRF was greater then 0.005, or the duty cycle was less than 75. For the chip rate detector and the radiometer, there was not a marked difference. In some cases, the DEF plus clipper increased the required S/N_o by 1dB, and in others it decreased the S/N_o by 1dB. Finally, for some cases the DEF plus clipper provided a decrease in the S/N_o required by the communication receiver for the desired BER. When the PRF was 0.05, the required S/N_o was reduced by approximately 3.5dB, and for a PRF of 0.10 the required S/N_o was reduced by almost 6dB.

PRF	Composite Quality Factor (dBs)		
	Chip-Rate Detector	MODAC	Radiometer
0.0005	3.02	18.02	1.02
0.0050	2.21	16.21	-0.79
0.0500	5.72	17.72	2.72
0.1000	6.19	6.19	3.19

(a)

PRF	Composite Quality Factor (dBs)		
	Chip-Rate Detector	MODAC	Radiometer
0.0005	3.02	6.02	-1.98
0.0050	3.21	6.21	-2.79
0.0500	6.72	8.72	1.72
0.1000	6.19	6.19	3.19

(b)

Table 5.4   Composite Quality Factor for Various PRF Values for (a) DEF (b) DEF with Clipping Blocks

	Composite Quality Factor (dBs)		
Duty Cycle	Chip-Rate Detector	MODAC	Radiometer
25	5.19	7.19	2.19
50	0.00	14.00	-4.00
75	-0.30	11.70	-6.30
100	-0.46	12.54	-5.46

(a)

	Composite Quality Factor (dBs)		
Duty Cycle	Chip-Rate Detector	MODAC	Radiometer
25	6.59	9.59	2.59
50	1.63	4.63	-3.37
75	4.17	5.17	-1.83
100	6.47	7.47	-0.53

(b)

Table 5.5 Composite Quality Factor for Various Duty Cycle Values for (a) DEF (b) DEF with Clipping Blocks

VI. Conclusion and Recommendations for Future Research

6.1 Conclusion

This thesis examined the effects of an excision filter upon the error rates and the detectability of a spread spectrum communication receiver in the presence of continuous wave and pulsed jammers. The communication system consisted of a direct sequence binary phase shift keyed transmitter, a direct sequence despreader, and a matched filter demodulator. The channel was assumed to be additive white Gaussian noise with no multi-path propagation. In addition, the jammer source consisted of complex tones with parameters which controlled the amplitude, duty cycle, and pulse repetition frequency. The interceptor models used were the basic wideband radiometer, the chip-rate detector, and the chip-rate detector with a noise reference (MODAC). The bit error rates of the communication receiver and the receiver operating characteristics of the interceptors were measured under twelve different pulsed and CW jammer scenarios. Finally, the bit error rates were measured as a function of the jammer frequency offset from the carrier frequency, the pulse duty cycle, and the pulse repetition frequency. These values were then used to evaluate the modulation quality factor and examine its behavior under various jamming conditions.

It was found that the excision filter used in this research worked very well in the presence of single and multiple CW jammers. The DEF was able to successfully locate and excise almost 100% of the jammer power. The BER curves obtained were consistent with the expected ideal results when the jammer was located at frequencies other than the carrier frequency. When the jammer was at the carrier frequency, the BER was degraded; however, the BER was still significantly lower than that obtained when no filter was present. The jammer power was chosen to obtain a jammer power to noise PSD ratio of approximately 27dB. This greatly exceeded the interference suppression capabilities of the DS-BPSK system and effectively rendered it useless ($P_e \approx 0.5$). However, the DEF did not perform quite as well in the presence of the pulsed jammers. The pulsed jammers, which occupy a larger

bandwidth, forced the DEF to remove a larger portion of the signal's spectrum. This resulted in higher BER values. These values, as for the CW jammers, were still acceptable compared to the performance of the system without the DEF. Finally, the curves obtained from the variation of the jammer parameters were consistent with the expected results.

The interceptors, when used with the DEF, also performed quite well in the presence of the CW jammers. However, the interceptors' performance was also degraded in the presence of the pulsed jammers. The reasons for this degradation are contained in Chapter 5. The modified DEF, consisting of the original DEF plus an amplitude limiting portion, was used in an attempt to overcome the degradation caused by the pulsed jammers. It proved to be fairly successful and showed a marked improvement in the ROC for the MODAC. In addition, it provided a decrease (approximately 6dB) in the E_b/N_o required by the communication receiver for the PRF values tested. However, these effects were not studied in depth and require further testing to be conclusive as to the overall benefits.

6.2 Recommendations for Future Research

There are three main areas of research that can be derived from this thesis effort. While all were addressed somewhat during the course of this thesis, they were not studied in depth and all require additional research. These three areas are

1. DEF Parameter Optimization and Threshold Calculation
2. Development of a More Effective Excision Filter
3. Examination of LPI Quality Factor

The first of these areas would concentrate on optimizing the DEF utilized in this thesis. The DEF has parameters which allow the user to change the FFT length, the type of window used by the data-prep block, and the threshold value used. For the simulations executed in this research, the FFT length was set to 256 points. This value was used as a trade-off between processing time and frequency localization of the filter. The relatively small vector size allowed for quick processing time; however, a larger vector length would allow for better frequency localization. By achieving better frequency localization, there

would be less distortion of the surrounding FFT bins, and the DEF would be able to remove the maximum amount of jammer without removing excessive amounts of the signal spectrum. The second parameter, the type of window used, also helped in frequency localization. For the simulations in this thesis, the rectangular window was used. Simulations executed by Lascody (7), who was also utilizing the DEF, indicated that a different window might help to better localize the jammer tone. For example, when a Hanning window was used, the jammer tone appeared to occupy a smaller bandwidth with less amplitude distortion in the amplitude of the signal spectrum. The Hanning window did produce distortion in the data signal; however, this distortion had little effect on the demodulator. It was still able to detect the data bits and successfully demodulate the signal. The combination of the FFT size and the window could possibly allow the DEF to better isolate the pulsed jammer tone. As stated earlier, this would allow for removal of the jammer with a minimum effect on the data's spectrum. The final parameter, the threshold, determined which FFT bins would be removed. The current DEF calculated the average signal value and increased it by the amount indicated by the threshold parameter. The main problem with this method was that the jammer signal was included in the calculation of the average value. This raised the threshold and decreased the ability of the filter to remove all of the jammer. If the threshold could be more accurately estimated to a level closer to the actual signal, more of the jammer signal could be removed.

The next area of possible research is the development of a more effective excision filter. The current DEF sets all FFT bins above the threshold to zero. If a method of approximating the data signal's spectrum was possible, the excised bins could be replaced with the approximated values corresponding to the region removed. One method that could be used would utilize the vector signal sink and vector signal source. By storing the vectors of the data signal to an ASCII file and averaging over the vectors for several data signals, an approximation to a signal's spectrum could be obtained. After the DEF detects a jammer and removes the bins which exceed the threshold, the excised bins could be replaced with the corresponding values from the approximate signal spectrum.

A final recommended area for future research extends the research done on the modulation quality factor and explores the remainder of the components of the LPI quality factor. By simulating a real-world system, the LPI characteristics could be fully tested. This would entail implementation of realistic transmission channels, which realistically duplicate atmospheric loss and distortion, and accurate antenna models. This would allow the effects of alternative antenna designs and interference suppression techniques to be quantified in respect to the maximum attainable communication range. In conjunction with this research, it could also be possible to optimize the intercept receivers. By finding the optimum filter bandwidths and observation periods, the modulation quality factor could also be determined with respect to different intercept receivers. In addition, the interference suppression quality factor could be derived for the DEF. This would allow the Q_{MOD} and Q_{IS} to be studied separately, eliminating the need for the emiprically derived Q_{COMP}.

Appendix A. LPI Quality Factors and Link Analysis
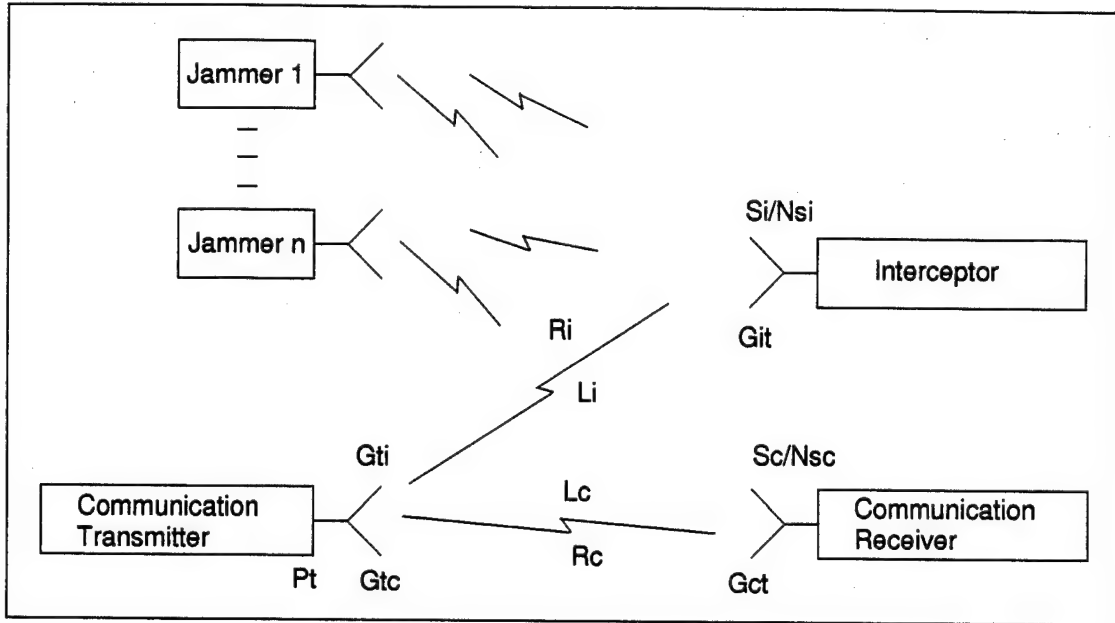
Figure A.1   LPI Scenario

A typical LPI scenario is shown in Figure A.1. In this scenario, a communication system attempts to successfully transmit information while being targeted by jammers and intercept receivers. The main objective of the communication system is to transfer the data while overcoming the jammers and avoiding detection by the interceptors. This can be done through the use of steerable antennas interference suppression filters, and coherent processing. The main parameters of the communication system are the E_b/N_o required to maintain a desired P_e, the transmit and receive antenna gains, and the receiver noise figure. These parameters determine the maximum communications range and intercept range, R_c and R_i, which can be achieved. The link budget analysis used to determine these quantities is found in (14). To derive the expression for R_c, we must determine the ratio of signal power to noise power density (note: noise power density is used instead of noise power to eliminate any constraints on the receiver bandwidth) that is available at the receiver. Assuming that a specific E_b/N_{sc} is required

A-1

to obtain a desired P_e, we can write

$$\frac{S_c}{N_{sc}} = \frac{E_b R_b}{N_{sc}} \qquad (A.1)$$

where E_b is the bit energy, and R_b is the transmitted bit rate. The signal power available at the receiver is found, through link analysis performed on Figure A.1, to be

$$S_c = \frac{P_t\, G_{tc}\, G_{ct}}{(4\,\pi\, R_c\, /\, \lambda)^2\, L_c} \qquad (A.2)$$

where

- P_t — transmitter power
- G_{tc} — gain of transmitter in direction of receiver
- G_{ct} — gain of receiver in direction of the transmitter
- $(4\,\pi\, R_c\, /\, \lambda)^2$ — is the free space propagation loss
- L_c — atmospheric losses

Next, the power spectral density of the noise and interference, N_{sc}, can be expressed as

$$N_{sc} = N_{oc} + N_{jc} \qquad (A.3)$$
$$= kT_{ac} + kT_o(F_c - 1) + \sum_{n=1}^{N} \sum_{m=1}^{M} g_{cn} g_{cm} \frac{J_{nmc}}{B_c} \qquad (A.4)$$

where

- k — Boltzmann's Constant
- B_c — communications receiver bandwidth
- T_{ac} — communications receiver antenna temperature
- T_o — thermal noise (290K)
- F_c — communications receiver noise figure
- N_{oc} — thermal noise power density
- N_{jc} — jammer power density
- g_{cn} — null steering antennas

- g_{cm} — adaptive interference suppression

In the above equation, the double summation and the J_{nmc} term account for the power spectral density of each discrete component of each jammer. It is assumed that there are N jammers each producing M discrete tones. On the J_{nmc} term, the subscript m represents the mth tone produced by the nth jammer. Substituting the expressions for S_c and N_{sc} into the expression for S_c/N_{sc} and solving for R_c, we obtain

$$R_c = \sqrt{\frac{P_t \, G_{tc} \, G_{ct}}{L_c \, N_{sc}} \left(\frac{\lambda}{4\pi}\right) \frac{1}{S_c/N_{sc}}} \qquad (A.5)$$

The next step is to obtain the expression for R_i, the maximum interception range. The main parameter in this analysis is the ratio of the signal power to noise power density that is available to the interceptor. R_i illustrates the maximum distance at which a desired P_F and P_D, for a given S_i/N_{si}, can be obtained. Using the same type of analysis as for R_c, we obtain

$$R_i = \sqrt{\frac{P_t \, G_{ti} \, G_{it}}{L_i \, N_{si}} \left(\frac{\lambda}{4\pi}\right) \frac{1}{(S_i/N_{si})}} \qquad (A.6)$$

where

- G_{ti} — gain of the transmitter in direction of interceptor
- G_{it} — gain of the interceptor in direction of transmitter
- L_i — atmospheric losses
- N_{si} — power spectral density of the noise and interference at the interceptor

We can then define the LPI quality factor (in decibels) to be

$$Q_{LPI} = 20 \, log \left(\frac{R_c}{R_i}\right) \qquad (A.7)$$

From this expression, it is obvious that an improvement in the LPI quality factor allows either a longer communications range or requires the interceptor to move closer to the communication transmitter.

In addition, the LPI quality factor requires that performance requirements for P_e, P_D, and P_F be established. These requirements will determine the S_c/N_{sc} and S_i/N_{si} that must be available to the receiver and the interceptor.

In order to maximize the LPI quality factor, the system designers have multiple options. They can use specialized antennas to control the antenna gains, use filters to reduce the interference entering their system, and specialized modulation schemes to achieve the desired P_e at a lower S_c/N_{sc}. As a means of quantifying these choices, the LPI quality factor can be expressed as

$$Q_{LPI} = Q_{ANT} + Q_{ATM} + Q_{IS} + Q_{MOD} \tag{A.8}$$

where

- Q_{ANT} is the Antenna quality factor
- Q_{ATM} is the Atmospheric quality factor
- Q_{IS} is the Interference Suppression quality factor
- Q_{MOD} is the Modulation quality factor

By performing trade-offs between system controlled parameters, the designers are able to maximize specific portions of the overall LPI quality factor. The invidual quality factors are discussed below.

A.1 Antenna Quality Factor

The antenna quality factor allows the designers to quantify the effects of antennas upon the system's performance. By utilizing high gain, low sidelobe antennas which possess a steerable beam, designers are able to minimize the amount of undesired interference while maximizing the amount of desired signal that enters a system. The antenna quality factor, in decibels, is given by

$$Q_{ANT} = 10 \, log \left(\frac{G_{ct}G_{tc}}{G_{ti}G_{it}} \right) \tag{A.9}$$

A-4

It is readily apparent that the communication system desires large values for G_{tc} and G_{ct} while having a small G_{ti}. At the same time, the interceptor desires a large G_{it}. While high gain narrow beam antennas can improve the antenna quality factor, there are trade-offs that must be considered. For example, a high gain antenna has a narrower bandwidth. This increases the interceptor's search and dwell time. The communication link on the other hand only requires more precise beam steering.

A.2 Atmospheric Quality Factor

The atmospheric quality factor is expressed by

$$Q_{ATM} = 10 \log \left(\frac{L_i}{L_c} \right) = \xi_i R_i - \xi_c R_c \tag{A.10}$$

where ξ_i is the transmitter to interceptor path loss, and ξ_c is the transmitter to receiver path loss (both quantities are in dB/Km). For most scenarios, the two path losses are assumed to be approximately equal.

A.3 Interference Suppression Quality Factor

The interference suppression quality factor, which quantifies the ability of the receiver and interceptor to suppress interference and noise, is expressed by

$$Q_{IS} = 10 \log \left[\frac{kT_{ai} + kt_o(F_i - 1) + \sum_{n=1}^{N} \sum_{m=1}^{M} g_{in} g_{im} \frac{J_{nmi}}{B_i}}{kT_{ac} + kt_o(F_c - 1) + \sum_{n=1}^{N} \sum_{m=1}^{M} g_{cn} g_{cm} \frac{J_{nmc}}{B_c}} \right] \tag{A.11}$$

It is obvious that if the communication receiver can successfully filter the interference and noise, it will increase the quality factor. At the same time, if the interceptor can accomplish the same task, it will reduce the quality factor. If both the interceptor and the receiver are successful at removing jammer interference, Q_{IS} is dominated by the receiver and interceptor noise figures and antenna noise temperatures.

A.4 Modulation Quality Factor

The modulation quality factor provides a figure of merit that is dependent upon only the type of modulation used and the type of interceptor encountered. It is expressed by

$$Q_{MOD} = 10 \, log \left(\frac{S_i/N_{si}}{S_c/N_{sc}} \right) \tag{A.12}$$

This quality factor compares the quality of communication, determined by P_e, with the quality of interception, determined by P_D and P_F. Any technique that decreases the amount of signal power required by the receiver will increase the quality factor. Examples of these techniques include error-correction coding and power density reduction.

Appendix B. **Block Code for Excisor**

B.1 **EXCISOR.C**

```c
#include "spw_platform.h"
#ifdef UNIX
#include "caedata/madlib/excisor/blockcode/excisoru.c"
#else
#ifdef VAX_VMS
#include "[caedata.madlib.excisor.blockcode]excisoru.c"
#endif VAX_VMS
#endif UNIX
static char *REVISION = "2.50";


/*
 *
 * Block Function: excisor
 * Library: madlib
 * Date: Mon Jul 31 16:42:40 1995
 *      Written By: James Lascody
 */
/**********************************************************************/
/*                                                                  */
/*    FEED_THROUGH_LIST INFORMATION:                                */
/*                                                                  */
/*    --> FEED_THROUGH_TYPE IS NOT EDITABLE. The BDE parameter      */
/*        screen associated with the block must be edited to change */
/*        the block's FEED_THROUGH_TYPE.                            */
/*                                                                  */
/*        FEED_THROUGH_TYPE = ALL_FEED_THROUGH.                     */
/*                                                                  */
/**********************************************************************/


/**********************************************************************/
/*                                                                  */
/*    LINK_OPTIONS INFORMATION:                                     */
/*                                                                  */
/*    --> The LINK_OPTIONS list is editable.  It contains all the   */
/*        libraries which the code must be linked to.  Each item in */
/*        the list must be surrounded by double quotes and          */
/*        separated by commas.  The math library is automatically   */
/*        linked, and does not need to be specified.  The paths     */
/*        may be specified as full paths or as paths relative to    */
/*        the host.                                                 */
/*        A link option can also be specified in the form "-lx"     */
/*        (where x is defined in the UNIX manual on "ld"            */
/*                                                                  */
/*        IMPORTANT:  The entire LINK_OPTIONS list must be deleted  */
/*        if it doesn't contain any elements.                       */
/*                                                                  */
/*        Sample LINK_OPTIONS list:                                 */
/*        (Actual list should be placed below this comment block)   */
/*                                                                  */
/*        LINK_OPTIONS = { "-lm",                                   */
/*                    "//host/code/lib/sample.a" };                 */
/*                                                                  */
/*                                                                  */
/**********************************************************************/


/**********************************************************************/
/*                                                                  */
```

```
/*      INCLUDE_DIRS INFORMATION:                              */
/*                                                             */
/*      --> The INCLUDE_DIRS list is editable.  The list should    */
/*          contain all directory search paths needed to locate all   */
/*          the include files used by this block.  It has the same    */
/*          format as the LINK_OPTIONS list.                   */
/*                                                             */
/*          IMPORTANT:  The entire INCLUDE_DIRS list must be deleted  */
/*          if it doesn't contain any elements.               */
/*                                                             */
/*          Sample INCLUDE_DIRS list:                          */
/*          (Actual list should be placed below this comment block)   */
/*                                                             */
/*          INCLUDE_DIRS = { "//host/u/code/include",          */
/*                          "//host/lib/dir" };                */
/*                                                             */
/*                                                             */
/***********************************************************************/


/***********************************************************************/
/*                                                             */
/*          EDITABLE FUNCTIONS                                 */
/*                  --> In_excisor_madlib ()                   */
/*                  --> Ro_excisor_madlib ()                   */
/*                  --> Te_excisor_madlib ()                   */
/*                                                             */
/*          Structure use:                                     */
/*            Typical input value reference                    */
/*              local_var = *(spb_input->var_name);            */
/* **OR**     local_var = I_var_name;       */
/*            Typical output value update                      */
/*              spb_output->var_name = local_var;              */
/* **OR**     O_var_name = local_var;       */
/*            Typical parameter reference                      */
/*              local_var = spb_parm->var_name;                */
/* **OR**     local_var = P_var_name;       */
/*                                                             */
/*          (See reference manual for further information)     */
/*                                                             */
/***********************************************************************/


/*
 *        Initialize Function (must be present)
 *        --> If editing, modify only the lines within the
 *            function's opening and closing brackets.
 *
 *        This function is used to initialize the state structure
 *            and constant outputs of the block.  It is called once
 *            for each block instance during simulation.
 *
 *        Function must always return either SYS_OK, SYS_TERM,
 *            or SYS_FATAL by using the return() function.
 *            User may modify the line containing "return(SYS_OK);".
 */

In_excisor_madlib (spb_parm, spb_input, spb_output, spb_state)
STRUCT Pt_excisor_madlib *spb_parm;
STRUCT It_excisor_madlib *spb_input;
STRUCT Ot_excisor_madlib *spb_output;
STRUCT St_excisor_madlib *spb_state;
{

return (SYS_OK);
}
```

```
/*
 *       Run Output Function (must be present)
 *       --> If editing, modify only the lines within the
 *           function's opening and closing brackets.
 *
 *       This function is used to update the outputs and/or state
 *           of the block.  It is called each iteration, for each
 *           block instance during simulation.
 *
 *       Function must always return either SYS_OK, SYS_TERM,
 *           or SYS_FATAL by using the return() function.
 *           User may modify the line containing "return(SYS_OK);".
 */

Ro_excisor_madlib (spb_parm, spb_input, spb_output, spb_state)
STRUCT Pt_excisor_madlib *spb_parm;
STRUCT It_excisor_madlib *spb_input;
STRUCT Ot_excisor_madlib *spb_output;
STRUCT St_excisor_madlib *spb_state;
{
 int i,n;
  double mag, avg_mag, Threshold;

/* This section calculates the average noise floor of the real and
 * imaginary FFT data.  Then the new threshold is set by adding the
 * desired excision threshold to the average noise level.
 */

  mag = 0.0;
  for (n=0; n< I_FFT_real_iovec_len; n++) {
   mag+=sqrt(I_FFT_real[n]*I_FFT_real[n]+I_FFT_imag[n]*I_FFT_imag[n]);
   }
  avg_mag = mag/(double)I_FFT_real_iovec_len;
  Threshold = avg_mag*pow((double)10.0,(double)(I_Threshold*0.1));
  O_Avg_Noise = Threshold;

/* This section compares the magnitude of the FFT to the threshold
 * and sets it to zero if the magnitude is above the threshold.
 */

 for (i=0; i < I_FFT_real_iovec_len; i++)
  {if (sqrt(I_FFT_real[i]*I_FFT_real[i]+I_FFT_imag[i]*I_FFT_imag[i])
>= Threshold)
      {  O_Excised_real[i]=0.000000000000001;
         O_Excised_imag[i]=0.000000000000001; }
       else {
         O_Excised_real[i]=I_FFT_real[i];
         O_Excised_imag[i]=I_FFT_imag[i]; }}


return (SYS_OK);
}

/*
 *       Termination Function (must be present)
 *       --> If editing, modify only the lines within the
 *           function's opening and closing brackets.
 *
 *       This function is used to dump the final state of the
 *           block.  It is called once for each block instance
 *           during the simulation.
 *
 *       Function must always return either SYS_OK, SYS_TERM,
```

```
*           or SYS_FATAL by using the return() function.
*           User may modify the line containing "return(SYS_OK);".
*/


Te_excisor_madlib (spb_parm, spb_input, spb_output, spb_state)
STRUCT Pt_excisor_madlib *spb_parm;
STRUCT It_excisor_madlib *spb_input;
STRUCT Ot_excisor_madlib *spb_output;
STRUCT St_excisor_madlib *spb_state;
{


return (SYS_OK);
}


/**********************************************************************/
/*                                                         */
/*      Add any additional functions you need here.           */
/*                                                         */
/**********************************************************************/
```

B.2   EXCISOR.H

```
#include "FBCDEFS.h"

/*
 *
 * Block Function: excisor
 * Library: madlib
 * Date: Mon Jul 31 16:42:40 1995
 *
 */


/**********************************************************************/
/*                                                         */
/*      EDITABLE USER DEFINED STATE STRUCTURE              */
/*               --> STRUCT St_excisor_madlib             */
/*                                                         */
/**********************************************************************/


/*
 * State Structure (User Defined, editable)
 */
STRUCT St_excisor_madlib {
int instance;
};


/**********************************************************************/
/*                                                         */
/*      UNEDITABLE SIMULATOR DEFINED STRUCTURES            */
/*               --> STRUCT Pt_excisor_madlib             */
/*               --> STRUCT It_excisor_madlib             */
/*               --> STRUCT Ot_excisor_madlib             */
/*                                                         */
/**********************************************************************/
/*
 * Parameter Structure, Simulator Defined, uneditable
 */
STRUCT Pt_excisor_madlib {
double Threshold;
double initial_value;
};
```

```
/*
 * Input Structure, Simulator Defined, uneditable
 */
STRUCT It_excisor_madlib {
long FFT_imag_iovec_len;
double *FFT_imag;
long FFT_real_iovec_len;
double *FFT_real;
double *Threshold;
};

/*
 * Output Structure, Simulator Defined, uneditable
 */
STRUCT Ot_excisor_madlib {
double Avg_Noise;
long Excised_imag_iovec_len;
double *Excised_imag;
long Excised_real_iovec_len;
double *Excised_real;
};

/**********************************************************************/
/*                                                              */
/*        The following #defines may be used to shorten         */
/*        references to members of the above structures.        */
/*                                                              */
/**********************************************************************/
#define P_Threshold (spb_parm->Threshold)
#define P_initial_value (spb_parm->initial_value)
#define I_FFT_imag_iovec_len (spb_input->FFT_imag_iovec_len)
#define I_FFT_imag (spb_input->FFT_imag)
#define I_FFT_real_iovec_len (spb_input->FFT_real_iovec_len)
#define I_FFT_real (spb_input->FFT_real)
#define I_Threshold (*spb_input->Threshold)
#define O_Avg_Noise (spb_output->Avg_Noise)
#define O_Excised_imag_iovec_len (spb_output->Excised_imag_iovec_len)
#define O_Excised_imag (spb_output->Excised_imag)
#define O_Excised_real_iovec_len (spb_output->Excised_real_iovec_len)
#define O_Excised_real (spb_output->Excised_real)
```

Appendix C. **List of Abbreviations**

AWGN   - Additive White Gaussian Noise

BDE   - Block Diagram Editor

BER   - Bit Error Rate

BPSK   - Binary Phase Shift Keying

BW   - Bandwidth

CW   - Continuous Wave

DEF   - Digital Excision Filter

DS   - Direct Sequence

FH   - Frequency Hopping

INFOSEC   - Information Security

LPI   - Low Probability of Intercept

PN   - Pseudonoise

PRF   - Pulse Repetition Frequency

PSD   - Power Spectral Density

ROC   - Receiver Operating Characteristics

SPW   - Signal Processing Worksystem

SS   - Spread Spectrum

TRANSEC   - Transmission Security

Bibliography

1. Balaban, Michael C. Jeruchim Philip and K. Sam Shanmugan. *Simulation of Communication Systems*. New York: Plenum Press, 1992.

2. Barnes, G.R. "Spread Spectrum Wireless Links," *Fourth European Conference on Radio Relay Systems*, 39–44 (October 1993).

3. Dixon, Robert C. *Spread Spectrum Systems*. John Wiley and Sons, 1984.

4. Falen, Gerald L. *Analysis and Simulation of Narrowband GPS Jamming Using Digital Temporal Filtering*. MS thesis, AFIT/GE/ENG/94D-09, School of Engineering, Air Force Institute of Technology (AU), Wright-Patterson AFB OH, December 1994.

5. Gottesman, Lynn D. and Laurence B. Milstein. "The Effect of a Narrowband Interference Rejection Filter on Coarse Acquisition in Direct Sequence Spread Spectrum," *Proceedings GLOBECOM '90*, 1:256–260 (1990).

6. Kuehls, John F. "Presence Detection of Binary-Phase-Shift-Keyed and Direct-Sequence Spread-Spectrum Signals Using a Prefilter-Delay-and-Mulitply Device," *IEEE Journal on Selected Areas in Communications*, 8(5) (June 1990).

7. Lascody, James A. *Narrowband Interference Supression in Spread Spectrum Communication Systems*. MS thesis, Air Force Institute of Technology, 1995.

8. Mills, Michael S. *Evaluation of an Acoustic Charge Transport Device For Adaptive Suppression in Spread Spectrum Communications Systems*. MS thesis, Air Force Institute of Technology, 1993.

9. Mills, Robert F. *Real-Time Digital Signal Processing Implementation for the Modulation Detection and Classification and Classification Receiver*. MS thesis, Air Force Institute of Technology, 1987.

10. Mills, Robert F. and Glenn E. Prescott. "A Comparison of Various Radiometer Detection Models." to appear in IEEE Transactions on Aerospace and Electronic Systems, January 1996.

11. Milstein, L. B. and P. K. Das. "An Analysis of a Real-time Transform Domain Filtering Digital Communication System - Part I: Narrowband Interference Rejection," *IEEE Trans. Comm.*, COMM-28:816–824 (June 1980).

12. Nicholson, David L. *Spread Spectrum Signal Design LPE and AJ Systems*. Computer Science Press, 1988.

13. Poor, H. Vincent. "Narrowband Interference Suppression in Spread Spectrum CDMA," *IEEE Personal Communications*, 14–27 (Third Quarter 1994).

14. Prescott, Glenn E. *Performance Metrics for Low Probability of Intercept Communication Systems*. Annual Technical Report, AFOSR/NM, Bolling AFB, Washington DC 20332-6448: Air Force Office of Scientific Research, October 1992.

15. Schoolcraft, Ralph. "Low Probability of Detection Communications - LPD Waveform Design and Detection Techniques," *MILCOM* (1991).

16. Shanmugan, K. Sam. "Simulation and Implementation of Communication and Signal Processing Systems," *IEEE Communications Magazine*, 25–53 (July 1994).

17. Sklar, Bernard. *Digital Communications Fundamentals and Applications*. Prentice Hall, 1988.

18. Taub, Herbert and Donald L. Schilling. *Principles of Communication Systems (Second Edition)*. McGraw-Hill, 1986.

19. Torrieri, Don J. *Principles of Secure Communication Systems*. Artech House, Inc., 1985.

Vita

Christopher B. Madden was born on 22 April 1972 at Tyndall AFB, Florida. In 1990 he graduated from Okawville Community High School in Okawville, Illinois. He received a Reserve Officer Training Corps scholarship and attended Parks College of Saint Louis University. In May 1994, he graduated Magna Cum Laude with a Bachelor of Science Degree in Electrical Engineering and was commissioned a Second Lieutenant in the U.S. Air Force. He was then assigned to the Air Force Institute of Technology at Wright-Patterson AFB to earn his Master of Science Degree in Electrical Engineering. After graduation, Lt. Madden will be assigned to Scott AFB where he will be a satellite engineer for the Air Force C4 Agency.

Permanent address: 27251 Will-Braden Circle
                     Athens AL 35611

REPORT DOCUMENTATION PAGE

Form Approved
OMB No. 0704-0188

1. AGENCY USE ONLY (Leave blank)	2. REPORT DATE December 1995	3. REPORT TYPE AND DATES COVERED Master's Thesis

4. TITLE AND SUBTITLE
Effects of Jamming and Excision Filtering Upon Error Rates and Detectability of a Spread Spectrum Communication System

5. FUNDING NUMBERS

6. AUTHOR(S)
Christopher B. Madden
2nd Lieutenant, USAF

7. PERFORMING ORGANIZATION NAME(S) AND ADDRESS(ES)
Air Force Institute of Technology
WPAFB OH 45433-6583

8. PERFORMING ORGANIZATION REPORT NUMBER
AFIT/EN/ENG/95D-13

9. SPONSORING / MONITORING AGENCY NAME(S) AND ADDRESS(ES)
James Stephens WL/AAWN-2
Bldg 620
2241 Avionics Circle Suite 16
WPAFB OH 45433-7318
(513)255-7007

10. SPONSORING / MONITORING AGENCY REPORT NUMBER

11. SUPPLEMENTARY NOTES

12a. DISTRIBUTION / AVAILABILITY STATEMENT
Approved for public release; Distribution Unlimited

12b. DISTRIBUTION CODE

13. ABSTRACT (Maximum 200 words)

This thesis examines the effects of a digital excision filter (DEF) upon the error rates and detectability of a Direct-Sequence Binary Phase Shift Keyed communication signal in the presence of both continuous-wave (CW) and pulsed jammers. Simulations were performed using the Comdisco Signal Processing Worksystem. Detector models used were the wideband radiometer and two forms of the chip-rate detector. Twelve jamming scenarios were used to test the performance of the DEF in the presence of the CW and pulsed jammers. In addition, the effects of the CW jammer frequency, the pulsed jammer duty cycle, and the pulsed jammer PRF were also examined. LPI quality factors were then used to quantify the performance of the DEF.

This research determined that the DEF was able to remove almost 100% of the CW jammer and allowed the communication receiver and interceptors to operate with little degradation. The DEF was less effective against the pulsed jammers; however, it still allowed the receivers to operate at an acceptable level for single jammers. When two or more pulsed jammers were present, the radiometer was still able to operate; however, the other interceptors' performance was unacceptable.

14. SUBJECT TERMS
Spread Spectrum, LPI, Signal Detection, Digital Excision Filtering, Communication System Simulation

15. NUMBER OF PAGES
101

16. PRICE CODE

17. SECURITY CLASSIFICATION OF REPORT UNCLASSIFIED	18. SECURITY CLASSIFICATION OF THIS PAGE UNCLASSIFIED	19. SECURITY CLASSIFICATION OF ABSTRACT UNCLASSIFIED	20. LIMITATION OF ABSTRACT UL